THE INDIAN RIVER INLET CABLE STAYED BRIDGE: THE EFFECT OF WIND SPEED AND DIRECTION ON ESTIMATES OF STAY CABLE FORCES

by

Shaymaa Khudhair Obayes

A thesis submitted to the Faculty of the University of Delaware in partial fulfillment of the requirements for the degree of Master of Civil Engineering

Summer 2017

THE INDIAN RIVER INLET CABLE STAYED BRIDGE: THE EFFECT OF WIND SPEED AND DIRECTION ON ESTIMATES OF STAY CABLE FORCES

by

Shaymaa Khudhair Obayes

Approved: ____

Harry W. Shenton III, Ph.D.
Professor in charge of thesis on behalf of the Advisory Committee

Approved: ____

Harry W. Shenton III, Ph.D.
Chair of the Department of Civil and Environmental Engineering

Approved: ____

Babatunde Ogunnaike, Ph.D.
Dean of the College of Engineering

Approved: ____

Ann L. Ardis, Ph.D.
Senior Vice Provost for Graduate and Professional Education

ACKNOWLEDGMENTS

I would like to thank Professor Tripp Shenton for his guidance and for being my advisor and thesis supervisor. I have learned a lot from his great personality and experience. Also, I would like to thank Dr. Chajes, for his advice in getting my thesis complete. I would like to express my special thanks to the members of the IRIB discussion group, our discussion helps me to know about so many new things I am thankful to them. and special thankful for Gary Wenczel for helping me in this research. My deepest gratitude to my friend Abu Nuwas, without his support it would have been difficult to finish my research.

Finally, to my love, and supportive husband, Isam: when the times got tough, your encouragement is much appreciated and noted. I would like to express my special thanks to my parents and brothers. Also, I would like to dedicate this thesis to my husband, children, and parents and my brothers. I cannot express enough thanks to them. For them all my love and gratitude for their continuous support and encouragement.

TABLE OF CONTENTS

Appendix

LIST OF TABLES

LIST OF FIGURES

ABSTRACT

The objective of this study is to estimate the tension in the stay cables of the Indian River Inlet bridge using measured cables vibrations in conjunction with dynamic cable theory. In addition, to evaluate the effect of the wind speed and direction on the ability to estimate the stay cable forces. A MATLAB script is developed to automate the data processing, using spectral density techniques to identify the cable natural frequencies and from these, estimate the tension. Making use of taut cable theory, which combines frequencies and tension force in a relationship, one can be extracted by relying on the other. The acceleration data that is considered for analysis purpose in this study is from two wind events: Winter Storm Jonas January, 23rd 2016, and Hurricane Matthew October, 9th 2016. The results show that the taut string theory is an accurate and straightforward method to estimate cable force by knowing the natural frequency of the cable. From the analysis work, it is seen that all the estimated tensions were approximately within the ultimate maximum and minimum ranges from the construction requirements with different percentages of no more than 15%. For average or gust wind speeds between 25 mph and 55 mph, the tension in the stay cables can be estimated without requirement for certain characteristics using taut cable theory. In addition, the directions from north or north-east for the wind data provide acceptable data for estimating the tension in the stay cables. moreover, there is not enough information to determine the validity of other directions to estimate tension for cables.

Chapter 1

INTRODUCTION

The popular thinking about construction is that buildings and bridges revolve around two aspects: building materials, such as mortar, brick, concrete and steel; and labor. Contrary to this, technology has had its impact on the construction field as it has on other areas of life. Compared to the past, technology is no longer dismissed or ignored; today it has a significant role in the construction industry that cannot be denied. In recent decades, many positive impacts of the use of technology in building construction have been acknowledged, such as ease of communication, surveillance, and monitoring systems. These positive effects can be seen in the Indian River Inlet Bridge where the monitoring system is easily accessed remotely.

The structural health monitoring system of the Indian River Inlet Bridge, which is the focus of this research, allows all parties involved to view the ongoing processes without travelling back and forth to the site. In addition, this modern system increases the collaboration and administrative activities of all the team members, which increases and ensures the safety of the bridge and the public. Structural health monitoring can provide fast and accurate responses to changes in the strain, displacement, and acceleration of the bridge, and how the changes affect the serviceability and sustainability of the bridge.

1.1 Bridge's History, Location and General Description

1.1.1 Bridge's History

In the first half of the 20th century, the popularity of Delaware's beach resort towns was growing, as was the number of automobiles purchased for personal use. This increased the urgency for construction of the Ocean Highway (State Route 1) between Rehoboth Beach, DE and Bethany Beach, DE. It also required the construction of a bridge to cross the Indian River Inlet.

Completion of work on the first bridge, which was made from a creosote timber trestle built in Newport, Delaware, was in 1934. This bridge was immediately affected by weather conditions, which led to its collapse. Six years later the Charles W. Cullen Bridge, a "swing bridge," was built of concrete and steel. The Charles W. Cullen Bridge was the official name of the bridge at that time. That bridge, which also collapsed because of the effects of ice flow, was replaced by another bridge in 1952. The life of that bridge was also short (Barnhart at el, 2012).

Despite the successive collapses of the bridges in this region, there was no surrender; the bridge was rebuilt. After several years, construction was completed on a new steel girder bridge. A twin span of the same design was built a few years later to handle the increase in traffic over the inlet. These structures served for many years, however, over time a serious scour problem developed around the main supporting piers of the bridge, which were located in the tidal inlet. The scour problem became so severe that yet another new bridge was commissioned. The previous designs impacted the contemporary one, which was started in 2008. It is obvious in the design of the new bridge that it can face all of the extreme weather conditions and erosion factors that lead to the demise of the earlier bridges. The current bridge opened in January 20, 2012. Figure (1.1) shows a recent photograph of the bridge.

Figure 1.1: Photograph of The Indian River Inlet Bridge

1.1.2 Bridge location

The bridge is located in Sussex County, Delaware, U.S.A (Figure (1.2)). It is located on State Route 1 and connects Rehoboth Beach and Bethany Beach, two very popular vacation and tourist towns in the state. The Delaware Department of Transportation (DelDOT) owns and maintains the Indian River Inlet Bridge. The bridge direction is 0°, 29’, 53.61” North.

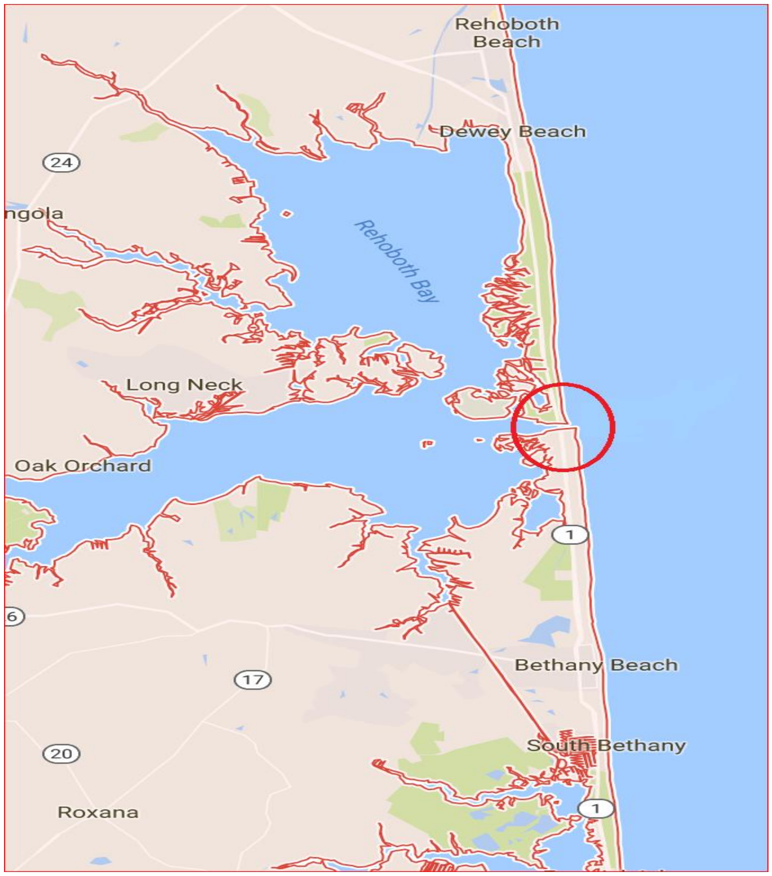

Figure 1.2: Indian River Inlet Bridge Location

1.1.3 General data and the layout of the bridge

The Indian River Inlet Bridge is a cable-stayed design, which is supported by four pylons (towers). It is 240 feet in height, and 19 pairs of cables are attached to each pylon (152 stay cables). The cables are rigged to the pylons in what is called a harp or parallel design, which is typical of cable stayed bridges. Figure (1.3) shows a harp design for a cable stayed bridge. With this design, all the stays have different lengths, the longest being the one that attaches near the top of the pylon. The total length of the bridge is 2,600 feet, and its width is 107.66 feet. The deck is divided into four traffic lines, a shoulder on each side, and a pedestrian walkway on the east side; their widths are 12 feet, 10 feet, and 10 feet, respectively.

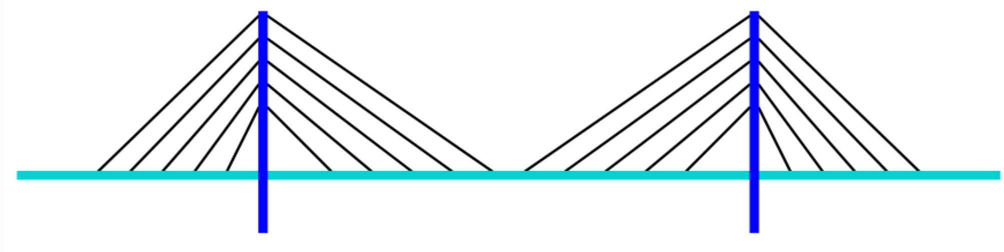

Figure 1.3: Harp Design for Cable-Stayed Bridge

As mentioned previously, there are 19 pairs of cables connected to each of the four pylons. Figure (1.4) and (1.5) show the bridge's north and south cable designations. The two pylons on the south end of the bridge are named 5E and 5W; the letter E and W denote the east and west side of the bridge, respectively. The two pylons on the north side of the bridge are denoted as 6E, which is located on the east side, and 6W, which is located on the west side. The stay cables are named based on the locations where they are anchored to the pylons. For example, to the south of pylon 5E are the stays 101E through 119E, and to the north of the pylon are stays 201E through 219E. To the south of pylon 6E are stays 301E through 319E, and the stays 401E through 419E are to the north of the pylon. The cables that are attached to the pylons on west side have the same designation as the cables on the east side except that the letter E is replaced by W. Figure (1.6) and (1.7) show the stay cable elevation in both north and south sides of the bridge, respectively.

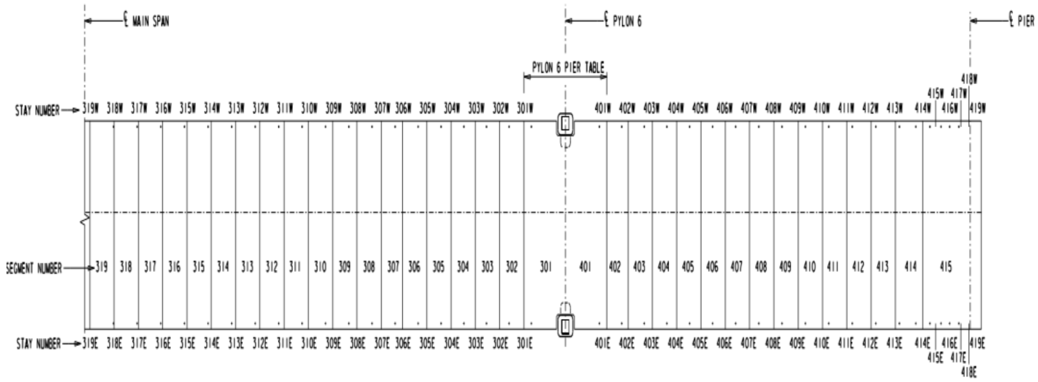

Figure 1.4: The North Plan of The Stay Cable Designation

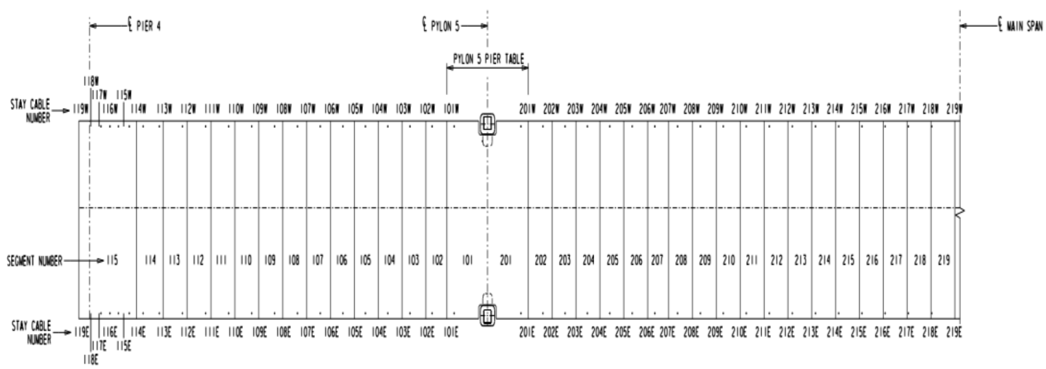

Figure 1.5: The South Plan of The Stay Cable Designation

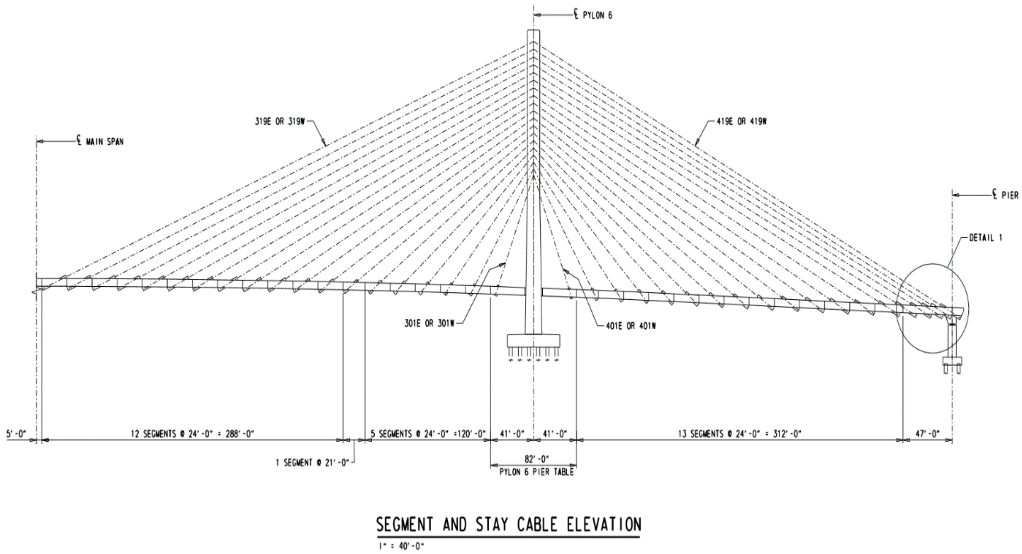

Figure 1.6: The Stay Cable Elevation in North Side of The Bridge

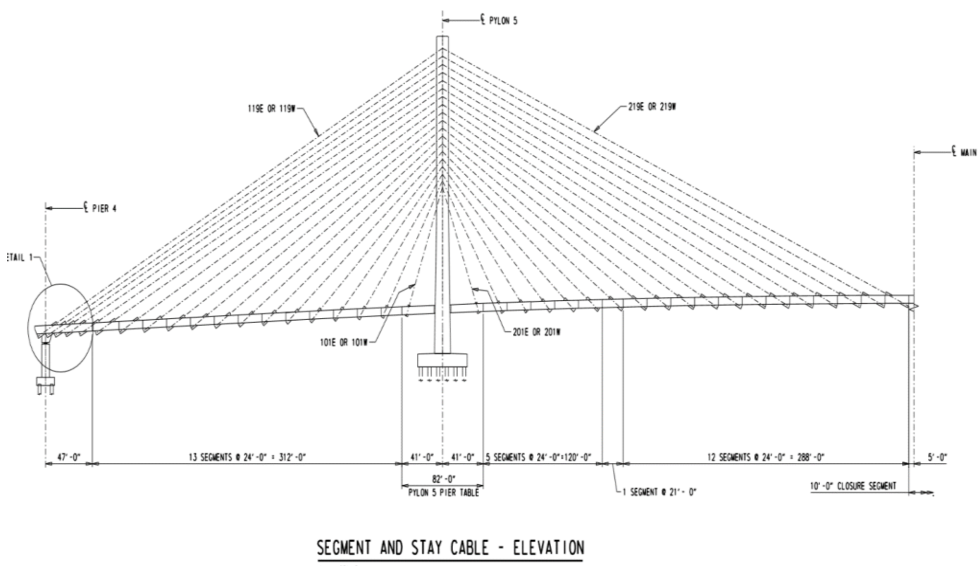

Figure 1.7: The Stay Cable Elevation in South Side of The Bridge

1.1.4 Cable Specification

The stay cable lengths vary from 505 feet to 95.2 feet, and each cable contains a different numbers of strands depending on the length. The longest, higher numbered stays that extend the furthest from the pylon, e.g., 119, 219, 319, and 419 have 61, 60, 60, 61 strands, respectively. The shorter, lower numbered stays that are closest to the pylons, e.g. 101, 201, 301, and 401, all have 19 strands. Each strand consists of 7-wires of low relaxation grade 270 ksi steel. The area of each strands is 0.2325 in2. According to the construction plans, the strand shall meet the requirements of ASTM A416 and will have a minimum ultimate capacity of 62.8 kip. Figure (1.8) shows a detailed cross-section of a typical stay. The HDPE tube that covers the stay is light blue in color, defined as RAL 5024. From the construction plans, the HDPE tube has to meet the requirements for stay pipes given in the PTI (Post-Tensioning Institute) "recommendations for stay cable design, testing and installation". (Construction drawing).

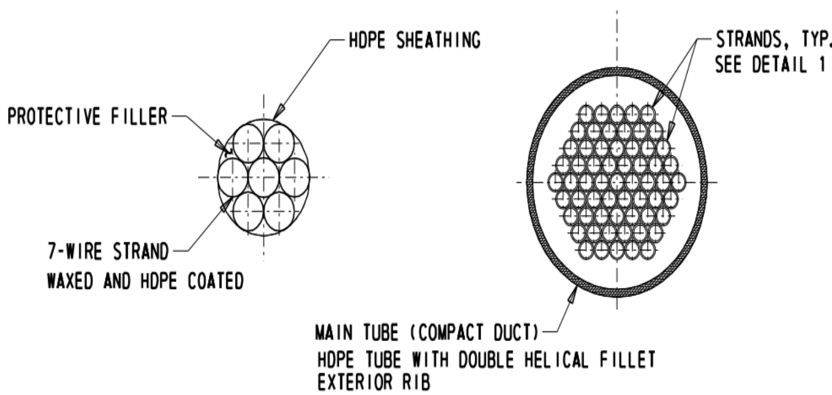

Figure 1.8: Cross-Section of The Strands and The Wires

The cable is passed through the pylon and held by an anchor block inside the pylon wall as shown in the Figure (1.9) (fixed pylon anchorage); the cable then passes through the deck inside an anchorage tube. Because the cable anchorage system is inside the pylon wall, it is susceptible to moisture and therefore corrosion. Thus, all the voids in the system are waxed.

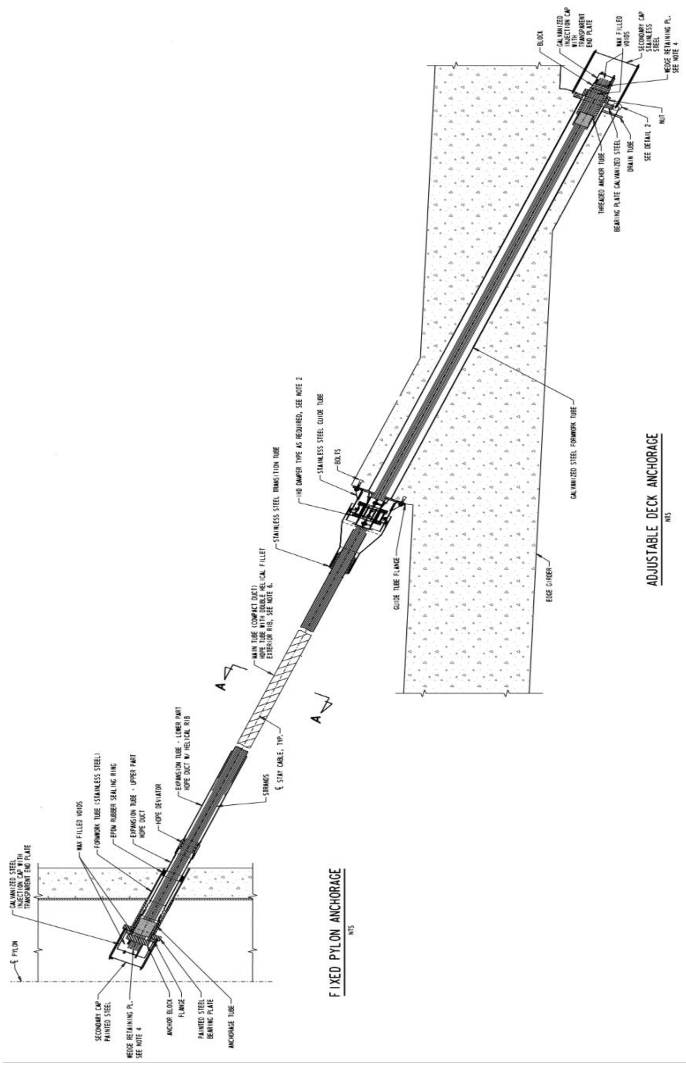

Figure 1.9: Stay- Cable Details

During the casting of the girder of the bridge, a galvanized steel formwork tube is cast into the girder to help anchor the cables. On the deck plane, there is an edge girder blister, through which all the strands enter. The stainless-steel transition tube and stainless steel guide tube guide the strands into the galvanized steel formwork tube through which the cable strands allow entry to the edge girder and stabilize there. The anchorage system at the deck contains a drain tube at the bottom to allow water that might collect there and cause corrosion to drain. Like the anchorage system at the pylon level, all the voids of the anchorage system at the deck level are waxed for the same reasons.

Due to the stay cable's intrinsic low damping, a circular internal hydraulic damper (IHD) has been used at the deck level above the anchorage system to increase the damping of the cable. The IHD will help to reduce the vibrations of the stay cable that might be caused by the effects of traffic or wind load. Because the Indian River Inlet Bridge cables have different length, mass, etc., the damping that is needed is different for each cable. For example, cable 119 requires a damping ratio 0.55 while stay 101 requires a damping ratio of 0.25. The different damping ratios are achieved by controlling a silicon oil with optimized viscosity that is inside the circular jack of the IHD.

1.2 Scope, Significance, and Objectives of The Research

In a cable-stayed bridge, the cables are a pivotal element of the overall structural system. Ideally, the tension in the stay cables should be monitored to ensure that no cable is overloaded and that the force does not exceed the design force of the cable. In addition, the cables are responsible for supporting the deck and transferring the load to the pylon, so any variations of the axial load in the cable may cause considerable influence on the global reaction of other parts of the bridge such as the deck and pylons.

There are several ways to measure the tension in the stay cables, whether at the end of the construction or during the life of the bridge. These methods can be based on "(i) the direct measurement of the stress in the tensioning jacks; (ii) the application of ring load cells or strain gauges in the strands; (iii) the measured elongation close to an anchorage; (iv) a topographic survey and (v) the indirect measurement of vibrations" (Caetano, 2007).

The direct method has an advantage that is the tension force in a cable can be measured directly using a hydraulic jack or a load cell. However, this method is impractical and requires considerable effort to jack each cable. In addition, heavy jacking equipment is needed which requires effort to install and operate. Using a load cell is another way to measure the tension force in the cable directly. However, typical load cells have a limited hole size, so if the cable has a large diameter this requires fabrication of a custom cell, which tend to be very large and can be expensive.

Therefore, an indirect method, which is based on measuring the transverse vibration (acceleration) of the stay cable is preferred. The measured accelerations of the cable can be transformed into the frequency domain by using a fast fourier transform. Once viewed in the frequency domain, the natural frequencies of the stay can be identified. Making use of the taut cable theory, which relates the tension in the cable to the cable's natural frequencies, the cable force can be estimated from the measured natural frequencies of the stay. This research will be focused on analyzing and calculating the tension force in the cables using taut cable theory.

At the Indian River Inlet Bridge, the acceleration data that can be used can be collected either through a pluck test or through measuring the ambient vibrations of the stays that are caused by traffic or light winds or during high wind events. Wind event and its effect on the tension forces of the stay-cables will be the scope of the research and will be explained in more detail in Chapter 4.

The objective of this research is to develop a quick, automated procedure for estimating the tension in the stay cables on the Indian River Inlet bridge using acceleration measurements of the stays during moderate to high wind events. In addition, to assess under what wind conditions (i.e., wind speed and direction), the estimates of cable force can be reliably determined.

1.3 Taut Cable Theory

The vibration of cables has been studied quite extensively over the years, much of which is reviewed in Chapter 2. This work has shown that in addition to the force carried by the cable, various geometric and material properties of the cable have an effect on the cable natural frequencies. The key properties can be categorized into four groups depending on the influence of sag-extensibility and bending stiffness: a) "neglects both sag-extensibility and bending stiffness". b) "takes account of the sag-extensibility without bending stiffness". c) "considers the bending stiffness but neglects the sag-extensibility," and d) "takes account of both sag-extensibility and bending stiffness" (Kim & Park, 2007).

Because the cables in stay cable bridges are typically characterized by their slenderness and length, the first category will be used and Equation (1.1) can be utilized to calculate the tension force in the cables. This equation is derived based on flat taut string theory.

$$T = 4mL^2 \left(\frac{fn}{n}\right)^2 \tag{1.1}$$

where: T: tension force in the cable (lb.)

m: mass per unit length (slug/ft)

L: length of the cable (ft.)

f_n: the nth natural frequency (Hz)

n: mode number

The above equation is applicable when the effect of sag-extensibility and bending stiffness can be neglected, which certainly facilitates the analysis. However, when the cable is not sufficiently tensioned, this equation does not yield a good result (Zui at all, 1996) and may introduce inaccuracies. The analysis and calculation of the tension force in the cables of the Indian River Inlet Bridge will be based on this equation. Further details about the derivation and the root of this equation are discussed in Chapter 2.

1.4 Thesis Outline

This thesis is divided into five chapters. Chapter 2 presents a literature review of cable dynamics and taut cable theory, which is the foundation of this work. The monitoring system, sensors details, data acquisition system, and the optimal sample rate for recording the stay cable acceleration data are discussed in Chapter 3. In Chapter 4 is presented the techniques and assumptions of the methodology of vibration data and the computer analysis method. The wind data that has been used in this research and the results and analysis from the wind data and the effect of the speed and the direction of the wind events on the estimated stay force are discussed in

Chapter 4 as well. Finally, Chapter 5 summarizes the findings of the study, presents conclusions, and offers suggestions for future research.

Chapter 2

LITERATURE REVIEW

The theory of a taut cable provides an approximate formula through which the tension force of the cable can be calculated based on measured vibrations, in a straightforward and accurate approach. From the 18th century to the present, the history of the theory of cable vibrations and taut string theory are reviewed in this chapter.

Brook Taylor, D'Alembert, Euler, and Daniel Bernoulli presented elements of the theory of vibration of a taut string during the first half of the eighteenth century. Both Bernoulli and Euler in 1732 and 1781, respectively, conducted their investigations on the transverse vibration of a uniform cable hanging under the effect of gravity that is supported at one end. They stated that an infinite series can be used as a solution for the natural frequencies of the cable. The investigation was further developed to first define Bessel's differential equation, which is now an important equation for solving many mathematical problems. During this time, the governing equation of motion for a continuously vibrating cable had not yet been developed and considerable effort had concentrated on discrete systems and had never extended to continuous systems. However, Lagrange in 1760 had solved the general equations of the motion of discrete systems. This equation appeared later in “Mecanique Analytique” in 1788 (Irvine & Caughey, 1974).

In 1820, Poisson contributed substantially to the existing body of work on the theory of cable vibrations. “The general Cartesian partial differential equations of the motion of a cable element under the action of a general force system” were given by

Poisson; who improved upon the previously developed solutions obtained by Fuss in 1796. However, the solution for the free vibration of a sagging cable was still unknown. In 1851, Rohrs and Stockes derived results for the symmetric vertical vibrations of a uniform suspended cable depending on a form of Poisson's general equations and "the equation of continuity of the chain" (Irvine & Caughey, 1974). Their solution was approximate, and was limited to a small sag-to-span ratio. Later, the exact solution was obtained by Routh in 1868 for an inextensible sagging cable; which is the same assumption that Rohrs presumed. The exact solution was for both symmetric and unsymmetric vertical vibrations of a cable. All of the studies mentioned so far concluded with a derivation of "an equation for the natural frequencies of a small-sag, inextensible, horizontal chain" (Triantafyllou and Grinfogel 1986). The same subject was discussed again by Rannie and Von Karman nearly sixty years later in 1941 and also by W. D. Rannie. Large sag of the cable was considered by Pugsley in 1949 for the ratio of the sag-to-span from 1:10 up to 1:4. Pugsley did his study on a semi-empirical theory for the natural frequencies of the cable, and he focused on the first three in-plane modes. Through this study, Pugsley clearly showed the applicability of the results as they related to the sag ratio. After this study, more accurate and satisfactory results were reached in cable dynamic theory again using inextensible cables by a group of researchers such as Saxon and Cahn (1953). All of the previous studies that had been done independently by Rudnick, Leonard and Saxon, Cahn and Saxon, and Pugsley show good agreement of the result when the sag-to-span ratio is 1:10 or greater (when this ratio approximates to zero, it will be smaller) (Irvine & Caughey, 1974). However, there was a discrepancy in the result when this ratio reduced to zero (the sag-to-span *(δ)* is the ratio of $s/l_{\circ}$ in Figure

(2.1)) for the inextensible cable, and the reason was unknown because of the lack of the theoretical and experimental study at that time. The point expressed by Irvine and Caughey, 1974, of this discrepancy was that inextensible cables are impossible. Because they failed to notice that the cable was stretched during the vibration in a symmetric mode, their standard analyses produced an inaccurate finding. Irvine and Caughey added, to elucidate a lack of compatibility, “a cable which has a very small sag to span ratio must stretch when vibrating with symmetric vertical motion. However, if the concept of inextensibility is adhered to, it must be concluded from the previous analyses that the classical, first symmetric vertical mode does not exist if even the slightest sag is present” (Irvine and Caughey, 1974). The significant support to the theory of cable vibrations happened in 1974 when Irvine and Caughey had done their research on the linear theory of free vibration; the cable ends are supported at the same level (horizontally) with sag-to- span ratio range from 1:8 to zero. The conclusion from this study was that “the natural frequencies of symmetric in-plane modes and the respective antisymmetric in plane modes” occur at the same time when the value of a parameter in which a dynamic behavior of the cable depends on reaching a ‘cross-over’ point (Starossek, 1994). Irvine enhanced and further improved the theory to include an inclined cable. However, this improvement was a modified version of the horizontal cable results. The linear theory Irvine expanded was based on the partial differential equation that was derived based on three assumptions:

1- the sag-to -span ratio << 1.

2- the vibration in x-direction is negligible, the vibration is only in xy-plane (Figure (2.1) shows the coordinates of the incline cable).

3- A quadratic parabola expresses the geometric shape of the inclination.

Equation (2.1) is the governing equation of motion in the y-direction (Zui et. al 1996).

$$\boldsymbol{EI}\frac{\delta^4 v(x,t)}{\delta x^4} - \boldsymbol{T}\frac{\delta^2 v(x,t)}{\delta x^2} - \boldsymbol{h}(\boldsymbol{t})\frac{\delta^2 y}{\delta x^2} + \frac{w}{g}\;\frac{\delta^2 v(x,t)}{\delta t^2} = \mathbf{0} \qquad (2.1)$$

where *EI* is the flexural rigidity of cable, *T* represents the constant axial force of the cable, *h(t)* is the time varying cable force due to the cable vibration, *w* and *g* are the weight of cable per unit length and gravitational acceleration, respectively, *v* is the deflection in the y-direction due to vibration, and *y(x)* is represented a parabolic shape of the cable.

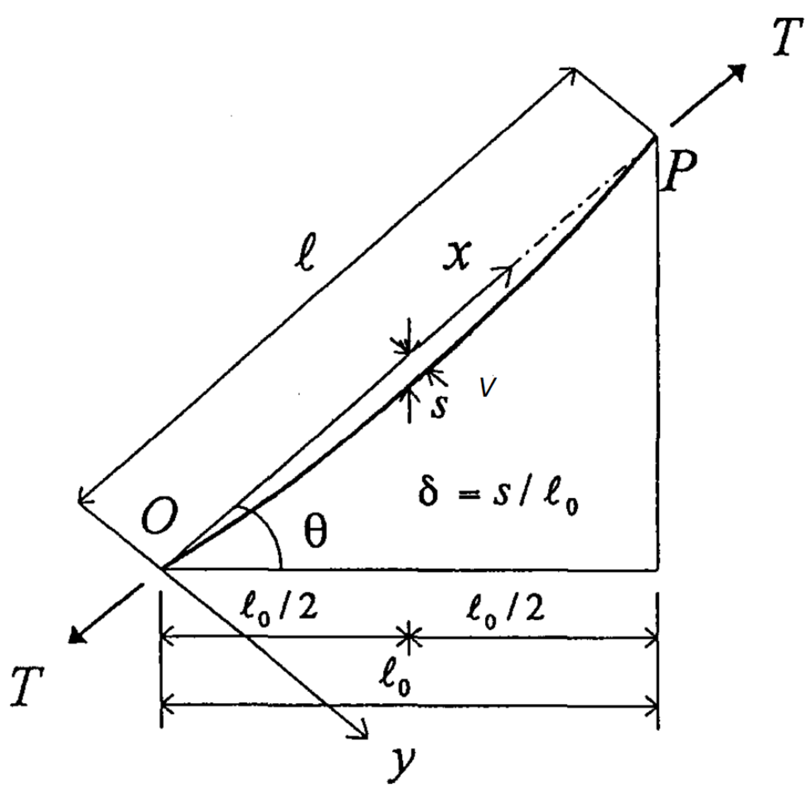

Figure 2.1: The Coordinates of The Incline Cable (Zui et. al 1996)

The additional derivative cable force from the vibration can be neglected even for small *T* for the second or higher order mode; however, *h(t)* cannot be ignored for the first-order mode (Zui et. al 1996). As mentioned in the previous chapter, the cable is characterized by its slenderness and length. Neglecting the bending stiffness and assuming *h(t)* is small for the second or higher order modes and can be neglected, Equation (2.1) becomes:

$$\frac{w}{g}\frac{\delta^2 v(x,t)}{\delta t^2} = T\frac{\delta^2 v(x,t)}{\delta x^2} \qquad (2.2)$$

which is the classical second order partial differential equation governing the response of a taut cable that is a function of just the mass of the cable and constant tensile force.

Irvine and Caughey in the paper that they published explained the solution of the Equation (2.2). In addition, Chopra, 2007 presents the solution for the equation of motion and the evaluation of dynamic response in his book *Dynamics of Structures*. Solving Equation (2.2) yields the expression for the natural frequencies of the cable.

$$f_n = \frac{n}{2L}\sqrt{\frac{Tg}{w}} \qquad (2.3)$$

where f_n is the theoretical value of the nth order natural frequency of a cable or string (Zui et. al 1996), and it is equal to $\frac{\omega}{2\pi}$, where ω is the nth natural circular frequency of the system. From Equation (2.3), an estimation of the tension force of a cable can be easily calculated by knowing the nth frequency of vibration.

Irvine and Caughey extended the theory to discover a fundamentally important equation of cable vibration theory. They obtained Equation (2.4) that shows a relationship between cable geometry and elasticity

$$\tan\left(\frac{1}{2}\boldsymbol{\beta l}\right) = \left(\frac{1}{2}\boldsymbol{\beta l}\right) - \left(\frac{4}{\lambda^2}\right)\left(\frac{1}{2}\boldsymbol{\beta l}\right)^3 \qquad (2.4)$$

Where - $$\boldsymbol{\beta} = \left(\frac{m\omega^2}{H}\right)^{0.5} \qquad (2.5)$$

$$\boldsymbol{\lambda}^2 = \left(\frac{8d}{l}\right)^2 \frac{1}{HL/EA} \qquad (2.6)$$

and $\boldsymbol{\beta l}$ represents to the particular (symmetric) vertical modal component (Irvine and Caughey, 1974), *d* is the sag of the cable, *H* is the tension force in the cable, *L* is the horizontal chord length of the cable, and EA specifies cross sectional stiffness of the cable. From the authors' experimental results, the value of the parameter $\boldsymbol{\lambda}^2$ has strongly influenced the natural frequency of the vibration of the cable. "It is clear that changes in the value of the characteristic parameter, $\boldsymbol{\lambda}^2$, caused substantial changes in the nature of the first symmetric in-plane mode" (Irvine & Caughey, 1974). Irvine & Caughey had reached from this study the validity of their theory which is that the inextensible cable $\boldsymbol{\lambda}^2$ value should be large enough; otherwise, an accurate solution will not be obtained using classical theory of the taut string (Equation (2.3)). Thus, this equation is effective in estimating the tension force in the Indian River Inlet Bridge cables because $\boldsymbol{\lambda}^2$ is small for the bridge, no more than 10-4. All the previous theories which assumed inextensible cables are valid for large $\boldsymbol{\lambda}^2$. A theory marked by exactness and accuracy of detail was given by

Triantafyllou in 1984 on inclined cables (Starossek, 1994). The same author in collaborating with Grinfogel after two years later had made valuable extension to the Irvine and Caughey investigation (Triantafyllou and Grinfogel 1986). Despite the great development that Irvine and Caughey added to incline cable vibration theory, the study did not reach such precision. It was simply because incline cables cannot have the same horizontal cables' properties. That was the main conclusion for Triantafyllou and Grinfogel's research.

Until the mid-nineties, all the investigations were about the linear theory of the cable dynamic; there was no extension to nonlinear theory. In 1996 Zui et al, made use of the modern cable theory and developed nonlinear equations that often must be solved numerically (Zui et al, 1996). In addition, they extended the study to include the effects of the inclination of the cable, bending stiffness, and the sagging ratio on the natural frequency of the cable. Back in 1980, Shinke et al. developed formulas depending on a parameter ξ which is equal to $\sqrt{(\boldsymbol{T}/\boldsymbol{E}*\boldsymbol{I})}$. (where *T* is the tension force of the cable, *EI* is the bending stiffness, and *l* is the length of the cable). The tension force can be estimated easily using those formulas, but not for a wide range of the parameter ξ. "The applicable range of the formulas is specified as $3 \leq \xi$ and $10 \leq \xi$ for the first and second modes of vibration, respectively" (Zui et al, 1996). For the investigation by Zui et al. on the same subject in 1994, the finding was simpler formulas valid for $200 \leq \xi$. Unlike the applicability of the equations in 1980, namely that "these formulas, however, have a certain limit of application and do not yield good results when the cable is not slender or not sufficiently tensioned", they had extended the applicability of their equation for any length and any internal force of the cable "as far as the vibration of first- or second-order mode is measurable" (Zui et al, 1996). The experimental result for different cables' length showed a good concurrence with practical result, which validated Zui et al's formulas.

In 2007, Kim and Park published a paper in which other cable parameters have been explained. As mentioned in chapter 1 and repeated here for convenience, there are four categories depending on considering the effect of "the sag-extensibility and bending stiffness": a) "neglects both sag-extensibility and bending stiffness". b) "takes account of the sag-extensibility without bending stiffness". c) "considers the bending stiffness but neglects the sag-extensibility". d) "takes account of both sag-extensibility and bending stiffness" (Kim & Park, 2007). Early in this chapter, Irvine derived the equation to estimate the tension force based on small sag ratio and neglecting the bending stiffness Equation (2.3). Solving this equation for tension yields:

$$\boldsymbol{T = 4mL^2 \left(\frac{f_n}{n}\right)^2} \qquad (2.7)$$

which was presented already in Chapter 1. This equation is valid for the first category defined by Kim and Park (2007). Considering the sag-extensibility in calculating tension force requires solving a nonlinear equation. Zui et al expounded the effect of the sag cable by deriving a dimensionless parameter Γ. They stated that for certain values of a variable Γ the sag and inclination cannot be neglected. The third classification is based on the beam theory and string theory. The tension force and flexural rigidity can be determined simply by using linear regression procedures (Kim & Park, 2007). Equation (2.8) is the formulation from beam theory to identify the tension force

$$\boldsymbol{T = 4mL^2 \left(\frac{f_n}{n}\right)^2 - \frac{EI}{l^2}(n\pi)^2} \qquad (2.8)$$

Finally, for both flexural rigidity and the sag ratio of the cable, Kim stated that "a prior knowledge of the axial rigidity and flexural rigidity of the target cable system is required." Because of the unavailability and invalidity of the flexural rigidity of the cable this category is not quite fully developed in Kim and Park's research. The authors' findings from this investigation highly support the Irvine and Caughey theory which is the estimation of tension force using taut cable theory for thin cables. In other words, taut cable theory is not authoritative for cables characterized by high flexural rigidity. The authors also conclude from their study that higher modes of the cable should be determined in order to use the linear regression approach for larger sag-span ratios.

From all the studies that have been done in investigating cable dynamics, and from all of the pervious discussions, it can be concluded that the taut string theory is an accurate and straightforward method to estimate cable force by knowing the natural frequency of the cable. Meaning that using Equation (2.7) to estimate the tension force in cables of the Indian River Inlet Bridge is accurate enough to depend on doing the analysis.

Chapter 3

MONITORING SYSTEM

The structural health monitoring system on the Indian River Inlet Bridge, which was designed by researchers at the University of Delaware, contains 150 sensors. The types of the sensors include accelerometers, strain gages, displacement transducers, and inclinometers. The data from the sensors are transmitted to a central monitoring system by a fiber-optic cable. Accelerometers, which will be the mean focus of this research, are used to measure the movement and vibration of the cable stays. In this chapter is presented a description of the sensors, their location on the bridge, data acquisition, and an analysis to determine the optimal sample rate for recording the stay cable acceleration data.

3.1 Instrumented Stay Cables

Of the 152 stay cables, only eleven are monitored: 219E, 319E, 319W, 315E, 310E, 310W, 305E, 404E, 408E, 413E, and 419E. To monitor all 152 cables would be impracticable because of the large amount of data that would be generated, the storage required, and the time needed to interpret of all the data. Thus, researchers at the University of Delaware selected 11 cables that would give a general indication of the behavior of most of the cables that were anchored to one pylon, and then a select few other cables on the bridge.

There are two stays on the west side and nine on the east side of the bridge that are monitored, and of the cables on the east side there is only one cable on the south end of the bridge that is instrumented. Figures (3.1) and (3.2) show the cables that are monitored on the south end of the bridge and north end of the bridge, with the cables labeled, respectively.

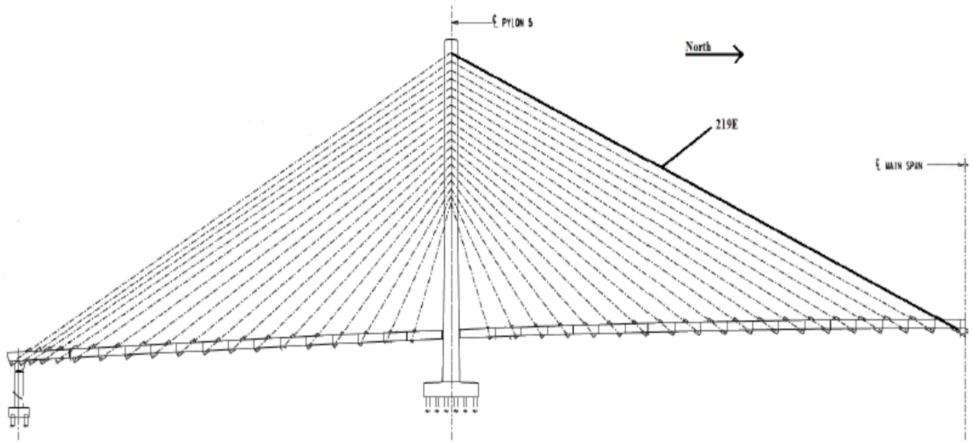

Figure 3.1: Cable Monitored on The South End of The Bridge

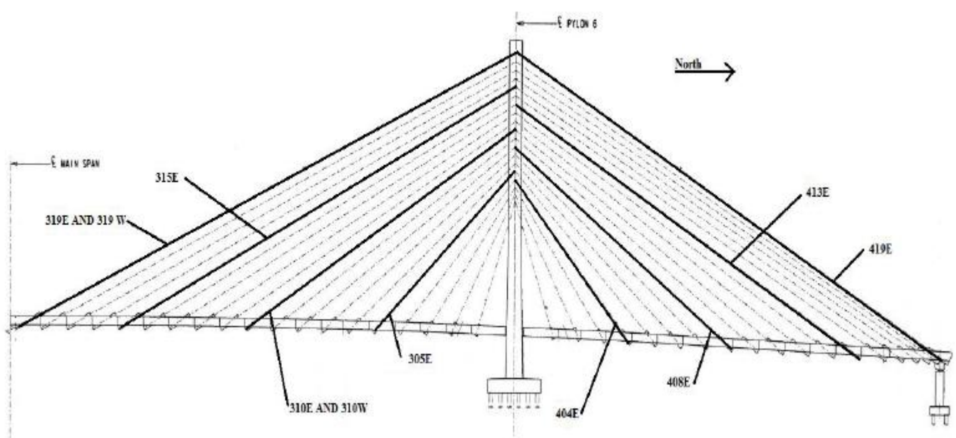

Figure 3.2: Cables Monitored on The North End of The Bridge

3.2 Sensor Locations and Designation

Figure (3.3) shows the accelerometers on the stays and their labels. All of the accelerometers are approximately 35 feet above the deck. Each sensor in the monitoring system has a unique designation, which is shown for the stay sensors in Figure (3.3), for easy reference to that sensor and its data. The first letter of the designation represents the sensors type, where "A" stands for accelerometer. The second letter ("Z" or "Y") denotes the direction in which the vibration of the cable is measured. The "E" or "W" denotes on which side of the bridge, East or West, the accelerometer is located, and finally, the numbers are the sequences of numbers for the accelerometers on the cable stays.

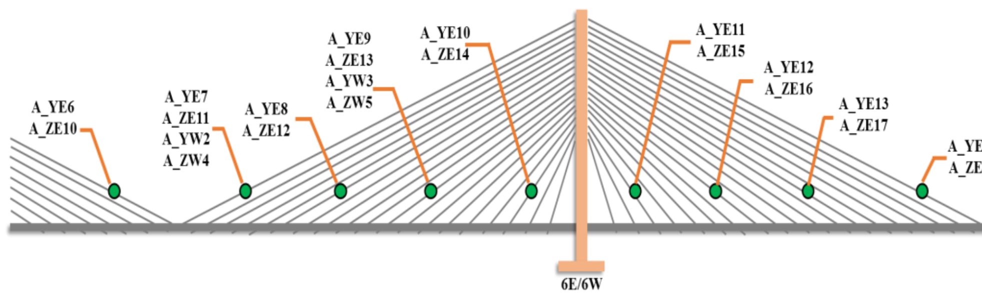

Figure 3.3: Elevation View of The Accelerometers

3.3 Data Acquisition System

A MicronOptics SM130 Optical Sensing Interrogator "sm - Sensing Module" is used to excite and interrogate the stay cable accelerometers (Figure (3.4)). It is also characterized by monitoring the dynamic sensors simultaneously and controlling static sensors with high resolution due to its high speed and excellent repeatability (Data sheet for Dynamic Optical Sensing Interrogator | sm130).

Figure 3.4: Micron Optical Sensing Interrogator | sm130

A computer connects to the SM130 by an Ethernet port and custom protocol, so it can receive the output wavelength data from the sensors. Also, it responds to the user commands of the optical interrogator core. The main features of the SM130 are that it has a wide wavelength range (standard 80nm and 160nm) to measure the sensing module, and many sensors per channel can be used with a high quality of operation because of using a spectral diagnostic view (Data sheet for Dynamic Optical Sensing Interrogator | sm130).

3.4 Sensor Specifications

The sensor that has been used on the Indian River Inlet bridge to measure acceleration is a Micron Optics model OS7100 sensor, which is shown in Figure (3.5). This sensor has a Patent Certification that “is covered under a US and International Patent Licensing Agreement between Micron Optics, Inc. and United Technologies Corporation”. The OS7100 sensor has been optimized for large structures and long term monitoring. Two single axis OS7100 sensors have been mounted to a specially fabricated mount to measure acceleration in two orthogonal directions on the stay cables, as shown in Figure (3.6). The accelerometer is designed “for outdoor installations on exposed structures” due to having a metallic body, armored cables, and weatherproof junction boxes, which provide good protection.

Figure 3.5: One Axis Micron Optics OS7100 Sensors

The accelerometer is attached to the stay cable by an assembly that includes 6” constant tension flexgear ring clamps, adjustment shafts, two rubber strips, and stay cable mounting bases as shown in Figure (3.6).

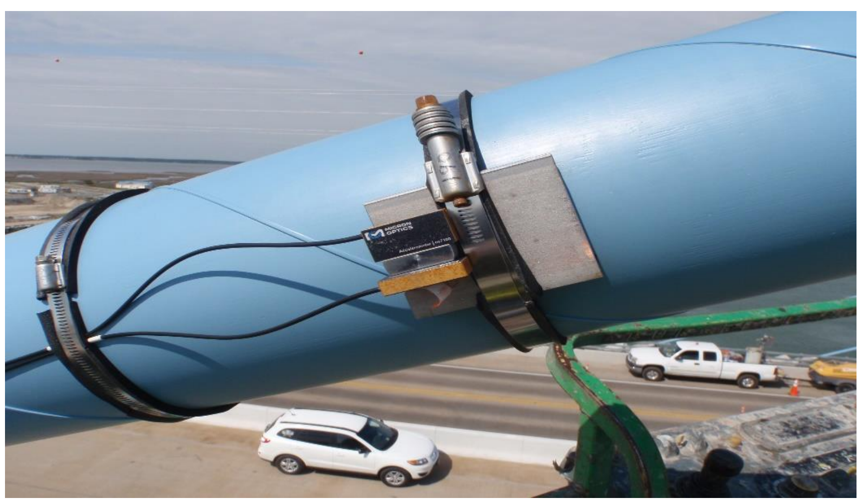

Figure 3.6: A Photograph for The Accelerometer

As shown in Figure (3.6) there are two OS7100 accelerometers attached on each stay to measure the vibration in two orthogonal directions. One sensor measures vibration in the Y- direction, which is perpendicular to the plane of the stays (east-west direction), and the other sensor measures vibration the in Z- direction which is in the plane of the stays and perpendicular to the stay. The positive Y-direction is toward the east and positive Z- direction is up.

3.5 Aliasing and the Selection of the Optimal Sample Rate

Measuring the acceleration of a continuous-time signal at regular time intervals is termed sampling, which is the procedure of transforming a continuous-time signal into a discrete-time signal (Rawat, 2015). Sampling slowly may not accurately display all of the information of a signal, and for this case, a faster sampling is required. However, sampling at a higher rate may cause a phenomenon called aliasing, which when viewed in the frequency domain, can create frequencies that do not exist in the input signal and may lead to an incorrect interpretation of the results. Aliasing happens when a high-frequency component in the spectrum of the input signal produces a replica, at a lower frequency in the spectrum (Rawat, 2015). It is a phenomenon that is created by the analog-to-digital conversion process. The sample rate is an important factor that needs to be considered in order to avoid aliasing.

The Nyquist frequency, which is equal to one half the rate at which a signal is sampled, (i.e., the sample rate) is the highest frequency that can be observed in the frequency domain of a measured signal. One method for eliminating aliasing is to use anti-aliasing filters. This is a low-pass filter put on the input signal to eliminate any frequencies above the filter cut-off frequency, which is usually set equal to one-half the sample rate (i.e., the Nyquist frequency) or just below it.

Equation (3.1) is a simple equation for calculating the value of an aliased frequency (National Instruments, 2006).

$$f_n = |f - Nf_s| \qquad (3.1)$$

where f_n is the aliased frequency, f_s is the sample rate, f is the frequency of the signal being sampled, and N is the closest integer to the ratio of the signal being sampled (f) to the sample rate (f_s). For example, suppose an 80 Hz signal is sampled at 100 Hz. In this case 80/100 = 0.8, which rounds to N = 1, therefore, |80 – 1*100| = 20 Hz. The 80 Hz (f=80 Hz) signal will fold down, about the Nyquist frequency, 100/2=50 Hz, and show up as a 20 Hz spike in the spectrum. Suppose a 260 Hz (f=260 Hz) signal is sampled at the same sample rate. In this case N=260/100=2.6, which rounds to 3 and the signal shows up at |260 – 3*100| = 40 Hz in the spectrum. Figure (3.7) shows the aliasing phenomenon. An anti-aliasing filter is designed to eliminate any frequencies above the cut-off frequency, usually the Nyquist frequency, so that they cannot fold down into the lower frequency range.

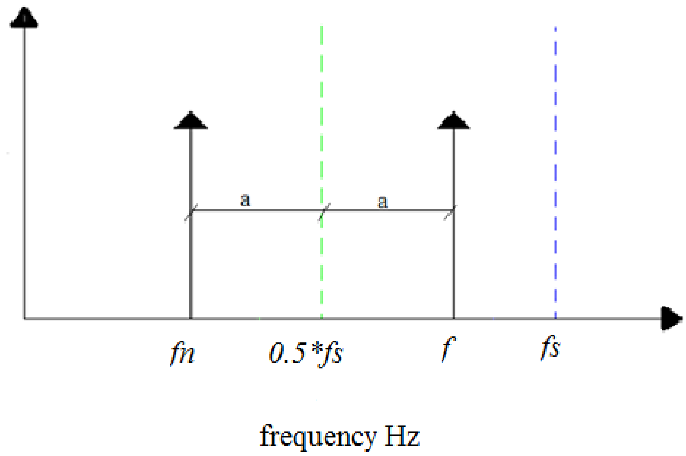

Figure 3.7: Aliasing Phenomenon

The Indian River Inlet bridge structural health monitoring system does not have anti-aliasing filters on the accelerometers, therefore, aliasing can be a problem. It was in fact found to be a problem soon after the system began collecting data and acceleration signals were analyzed in the frequency domain. Specifically, the spectra for the stay cable accelerometers were overwhelmed in the low frequency range (i.e, 0 to 10 Hz range) by a very dominate spike in the spectra. This made it very difficult to identify the natural frequencies of the stay cables themselves. After much investigation, this spike was attributed to the natural frequency of the sensor itself, being aliased and folding down into the low frequency range (Davidson, 2013).

When the accelerometers are sampled at too low of a rate, the natural frequency of the sensors, which is the aliased frequency *(f)* in Equation (3.1), will fold into the low frequency range and make identifying the stay natural frequencies very difficult, as will be shown later in this section. One option for eliminating this problem is to sample the accelerations at a very high rate, e.g., above 500 Hz. However, this produces significantly more data that must to be post-processed, and because of hardware limitations of the sm130, the number of sensors that can be monitored simultaneously decreases as the sample rate increases. The other option is to determine an optimal sample rate that pushes any aliased frequencies out of the low frequency range where the stay natural frequencies are expected to be found (i.e., 0 to 10 Hz), but that is still fast enough to sample all of the stays simultaneously. To do this requires knowing the approximate natural frequency of the mounted sensors.

The manufacturer's stated frequency range of the OS7100 is DC to 300 Hz. MicronOptics does not measure the actual natural frequency of their accelerometers, but states that they are in the range of 700 Hz. To identify the natural frequency of the sensors, so that the sample rate used for normal sampling of dynamic data could be optimized, stay cable accelerations were collected on the bridge during Hurricane Arthur on July 4th 2014. The duration of the data was 10 minutes and the sample rate was 1000 Hz, well above the assumed natural frequency of the mounted sensors. Figure (3.8) shows an example of the power spectra for cable 319E from the data that was recorded for the Y-direction sensor with a sample rate of 1000 Hz. The power spectrum of the recorded data was generated using the MATLAB script that will be discussed in more detail in Chapter 4. As can be seen from Figure (3.8), there is a spike at 264.4 Hz: this represents the aliased frequency, which is the sensor natural frequency that has folded down below the Nyquist frequency of 500 Hz. Notice that there is a cluster of spikes below 10 Hz that are the stay cable natural frequencies. According to Figure (3.7), the distance from the spike to 500 Hz (a in Figure 3.7) for this sensor is 235.6 Hz, so the natural frequency of sensor A_YE7 is equal to 500+a which is 735.6 Hz. This process was repeated for all sensors using data that was sampled at 500 Hz. The natural frequencies were then confirmed by using the same process to predict the aliased frequency in data that was sampled at 250 Hz. The remaining power spectra plots for other sensors are shown in Appendix A.

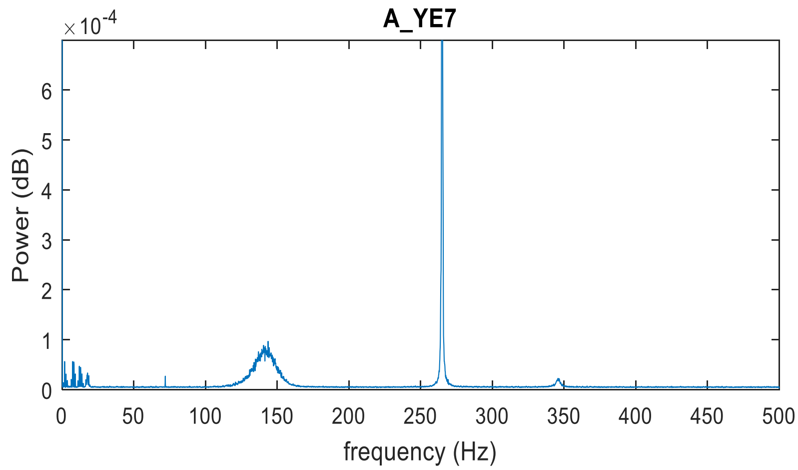

Figure 3.8: Wind Event Data for 319E (Y-Direction)

There is a wide band between 120-170 Hz in the power spectra for almost all of the stay cable accelerometers. That is not thought to be a natural frequency of the sensors or the stays: there is no immediate explanation for what this is in the spectra. However, as mentioned earlier, anti-aliasing filters are not used in the monitoring system, thus, any other higher frequencies might fold down and materialize as a lower frequency in the spectra. There are many factors that might be responsible for creating false frequencies in the spectra and folding them from their normal values, such as electronic effects and coupled vibrations. Not cutting off all of the undesired frequencies is a problem for estimating the tension in the stay cables, so using anti-aliasing filters to allow passing only appropriate frequencies in the input data is important and influential for accurate tension force. However, because the natural frequencies of the stay cables themselves are in the 0-10 Hz range, the wide band signal between 120-170 Hz is not considered a problem.

Using Figure (3.8), similar plots in the appendix, and the result from the data analysis, the natural frequency of the accelerometers have been calculated. Table (3.1) shows the estimated natural frequencies of the sensors (column 4). Note that the natural frequencies of sensor A-YE6, could not be detected and therefore are denoted as “None” in the table. (see the first figure in the Appendix). And there is no data recorded for sensors A-YE11 and A-ZE15.

Table 3.1: The Natural Frequency of The Accelerometers

Stay	System Gauge Designation	Frequencies in Power Spectra (Hz)	Estimated Sensor Natural Frequency (Hz)
219E	A-YE6	None	None
	A-ZE10	280.8	719.2
319E	A-YE7	264.4	735.6
	A-ZE11	260	740
319W	A-YW2	275.3	724.7
	A-ZW4	253.7	746.3
315E	A-YE8	285.4	714.6
	A-ZE12	270.5	729.5
310E	A-YE9	249.4	750.6
	A-ZE13	268.1	731.9
310W	A-YW3	260.4	739.6
	A-ZW5	259.4	740.6
305E	A-YE10	257.1	742.9
	A-ZE14	265.3	734.7
404E	A-YE11	None	None
	A-ZE15	None	None
408E	A-YE12	228.1	771.9
	A-ZE16	245.7	754.3
413E	A-YE13	262.3	737.7
	A-ZE17	245.1	754.9
419E	A-YE14	250.5	749.5
	A-ZE18	251.2	748.8

With estimates of the mounted natural frequencies of all of the stay accelerometers it is now possible to determine an optimal sample rate for collecting “high speed” data, that will minimize the effects of aliasing. The goal is to determine a sample rate that pushes any aliased frequencies out of the low frequency range of the spectrum, where the natural frequencies of the stay cables are expected to be found (i.e., the 0-10 Hz range). The values in Table (3.1) show that the natural frequencies of the sensors are between 710 and 755 Hz. Using these natural frequencies as an original frequency *(f)* in Equation (3.1), and varying the sample rate f_s from 50 to 280 Hz, the aliased frequencies were computed. The sample rate that provides the best compromise between the need for sampling accelerations fast enough, and not having spectra in the low frequency range swamped by aliased frequencies, is 167 Hz. This is the sample rate that has been used to sample the stays going forward.

Chapter 4

VIBRATION DATA AND ANALYSIS METHODS

In this chapter, the computer analysis method that has been developed to analyze the acceleration data to determine the natural frequencies of the stay cables, and then the tension in the stays, is presented. This chapter focuses on detailed analysis of the data from two wind events, the data from Winter Storm Jonas, January 23rd, 2016 and Hurricane Matthew October, 9th 2016. Finally, the effects of the wind speed and direction on the ability to estimate the stay forces is presented.

4.1 Tension and Theoretical Natural Frequencies of the Stays

Table (4.1) shows the properties of the stay cables. Column one represents the cable designation; the second column shows the length *(L)* of each cable. The *m* in Equation (1.1) is listed in column 3, which is the mass per unit length of the cable. The last column shows the percent of the minimum damping ratio that should be provided by the dampers.

Table 4.1: Cables Details

Stay (1)	Length (ft) (2)	Linear Mass (slug/ft) (3)	Minimum Design Damping (%) (4)
219E	505	1.4725	0.59
319E	505	1.4752	0.59
319W	505	1.4752	0.59
315E	407.4	1.0081	0.51
310E	287	0.8852	0.41
310W	287	0.8852	0.41
305E	171.7	0.6147	0.31
404E	154.8	0.5901	0.3
408E	246.6	0.8114	0.37
413E	367.3	0.9343	0.47
419E	458.9	1.4999	0.55

Table (4.2) shows the estimated (design) tension at the end of construction (EOC) and 10,000-day end of construction for each of the instrumented cables (obtained from construction drawings). This table also lists the cable tension that was measured by the contractor using a hydraulic jack, in December of 2011, when the stays were jacked to their final position. The design and measured tension can be used to calculate the natural frequencies of the cables for each mode number using Equation (1.1). The natural frequencies obtained from the acceleration data during the wind event will be compared to these "theoretical" natural frequencies. Tables (4.3) and (4.4) show the natural frequencies of the cables based on the design EOC tension and the contractor measured tensions, respectively.

Table 4.2: Design and Contractor Measured Tension for Monitored Cables

Stay	Estimated Design EOC Tension (kips)	Estimated Design 10,000 Days Tension (kips)	Contractor Hydraulic Jack Measured Tension (kips)
219E	1438	1517	1439
319E	1432	1534	1386
319W	1390	1491	1387
315E	768	822	767
310E	758	836	895
310W	758	836	872
305E	576	608	578
404E	491	511	561
408E	688	736	725
413E	934	970	885
419E	1127	1254	1225

Table 4.3: Theoretical Natural Frequencies from Estimated Design End of Construction (EOC) Tensions

Stay	Estimated Natural Frequency (Hz)					
	Mode Number					
	n=1	n=2	n=3	n=4	n=5	n=6
219E	0.978	1.956	2.933	3.910	4.888	5.865
319E	0.975	1.951	2.926	3.902	4.878	5.853
319W	0.961	1.922	2.883	3.844	4.804	5.766
315E	1.071	2.143	3.214	4.285	5.356	6.427
310E	1.612	3.224	4.837	6.449	8.056	9.673
310W	1.611	3.222	4.833	6.444	8.056	9.667
305E	2.819	5.638	8.457	11.276	14.095	16.913
404E	2.946	5.893	8.839	11.785	14.731	17.678
408E	1.867	3.734	5.601	7.468	9.335	11.202
413E	1.361	2.722	4.083	5.444	6.805	8.166
419E	0.944	1.889	2.833	3.778	4.722	5.667

Table 4.4: Theoretical Natural Frequencies from Contractor Hydraulic Jack Tension

Stay	Estimated Natural Frequency (Hz)					
	Mode Number					
	n=1	n=2	n=3	n=4	n=5	n=6
219E	0.978	1.956	2.934	3.911	4.889	5.867
319E	0.960	1.919	2.879	3.839	4.798	5.758
319W	0.960	1.920	2.880	3.840	4.800	5.760
315E	1.071	2.141	3.212	4.282	5.353	6.423
310E	1.752	3.504	5.255	7.007	8.759	10.511
310W	1.729	3.458	5.188	6.917	8.646	10.375
305E	2.824	5.648	8.471	11.295	14.119	16.943
404E	3.149	6.299	9.448	12.597	15.756	18.896
408E	1.992	3.833	5.750	7.666	9.583	11.499
413E	1.420	2.841	4.261	5.682	7.102	8.522
419E	0.985	1.969	2.954	3.939	4.923	5.908

4.2 Analysis Methods

4.2.1 Fourier Transform Analysis Method

Using Fourier series to analyze periodic phenomena was first introduced in Fourier analysis, which then developed to Fourier transform. Fourier transform is concerned with analyzing nonperiodic phenomena (Bracewell, 1986). By considering the nonperiodic phenomena, the spectrum signal which is the result of transforming a discrete set of frequencies in the periodic signal into the nonperiodic signal will be created. Hence, this spectrum can be analyzed in the frequency domain or even time domain ((Bracewell, 1986). In addition, the Fourier transform is a fundamental transform in frequency analysis. Acceleration power spectral density versus frequency can be obtained from transforming the data into the frequency domain (Rogers at el, 1997). For a large data set, such as the data from the accelerometer sensors on the Indian River inlet bridge, using the power spectra of the acceleration data is a much easier method. In any data, the dominant frequency components can be indicated using a frequency domain function that is the power spectral density (Rogers at el, 1990). Moreover, "The power spectral density function represents how the mean square value of a time function is distributed over the infinite frequency range" (Rogers at el, 1990). The more dominant frequency in the cables vibration is that which has a higher power in the time history because the power spectral density represents the power of the signal. Thus, the data that can be obtained from the sensors in the time domain can be used to determine what the more dominant natural frequencies of a cable are.

4.2.2 Data Processing to Determine Estimated Stay Tension

The most significant task of long-term structural health monitoring is analyzing and processing the large amounts of data that are recorded. During just two wind events at the Indian River Inlet bridge, approximately 18 hours of data have been recorded at a sample rate of 167 samples-per-second. The data are stored in 108 data files. Each record is ten minutes long; each data file will result in up to 100,200 readings per sensor. It is difficult to manually process each file individually with this large amount of data. Thus, an automated procedure is necessary to analyze these large data files. The MATLAB software has been used to analyze acceleration data; a script file was created to process the acceleration data files automatically and extract the natural frequencies and tensions of the stay cables.

The MATLAB command "pwelch" is used to calculate the power spectral density of a data set. The "pwelch" command returns the power spectral density (PSD) estimate of the input time history and a vector of cyclical frequencies (f). The PSD estimate is a positive real value. The cyclical frequencies are also positive real-valued and span the interval between zero and the sample rate divided by two (i.e., the Nyquist frequency). The units of the PSD depend on the units of the input data: the unit of the PSD estimate is the square magnitude unit of the time history data, per the frequency unit (MathWorks, 2012).

After processing the acceleration data with the pwelch command, plots are created of PSD versus frequency. Dominant frequencies of the input time history will show as a peak in the PSD. Hence, the fundamental frequencies of the cable will be the peaks over the domain.

Figure (4.1) shows an example of a two-sided power spectral density (MathWorks, 2012). The power spectral density shown in Figure (4.1) is the output from a signal consisting of a 100 Hz sinusoid, and the sample rate that has been used is 1 kHz for 5 seconds in duration. By using Welch's method and processed through a

MATLAB program, the power spectrum is obtained. It can be seen from the figure the dominant frequencies are at -100 and 100 Hz.

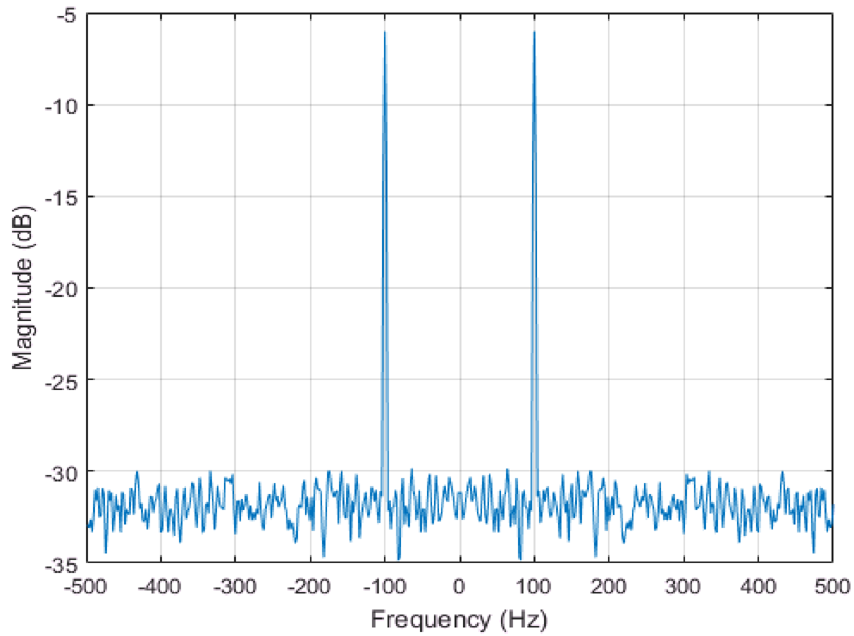

Figure 4.1: A Power Spectral Density

There are various input parameters to the MATLAB “pwelch” function that control how the data is processed and the PSD is computed. The key parameters that have been used to analyze the wind event data are the “window”, “noverlap”, and “sample rate” parameters. The “window” value is an integer number that defines the length of the vector that is processed. The function breaks the input data into n segments of length “window”, computes the PSD of each one separately, and then computes the average of the n values at each frequency in the spectra. In this analysis, the window length is 8,192. “Noverlap” is an integer number that describes the number of overlapped samples, which can be anything between zero and the length of the window minus one. With this parameter the segments are overlapped, producing many more PSD's of the input signal that are then averaged, which usually yields a better average measure of the PSD of the input data. In this analysis the overlap is equal to 4,096 (one half the window length). The "sample rate" is set equal to the sample rate of the recording, 167 samples-per-second (Hz).

With the PSD of a stay computed, the next step is to identify all of the local maximum peaks in the spectra using the MATLAB command "findpeaks." A local peak is one that is larger than its two neighboring samples: some of the identified peaks are natural frequencies of the stay, and some are not. Because of the low damping of the cables, "their Fourier spectra are characterized by high and sharp modal peaks" which are the frequencies of the cables (Cho at el, 2010). The process continues with identifying the fundamental frequency of the stay, which is assumed to be located between 0 and 3 Hz (Tables (4.3) and (4.4)). The fundamental frequency is identified by calculating the average all of the peaks and then using a threshold times the average as a limit, which the fundamental frequency must be greater than. Whenever a peak closet to the theoretical fundamental frequency of the cable that is more than this limit is identified, it will be designated the estimated fundamental frequency for that cable.

With the fundamental frequency identified, a search for the next five natural frequencies of the stay begins. Knowing that theoretically the natural frequencies of the stay should be integer multiples of the fundamental frequency, the algorithm uses this information to search for the other frequencies. Equation (1.1) shows that there is a direct proportion between the fundamental frequency and higher frequencies. This proportion is that the ratio of the second to the first, the third to the first and so on, is equal to an integer number *n*. For example, the second mode is two times the first mode (Cho at el, 2010). This pattern or ratio is used in the procedure to identify the stay frequencies from all of the potential peaks identified in the PSD that are 20% more than or less than a multiple integer of the fundamental frequency. Only those frequencies with a green dot follow this pattern, and therefore, only these are used to calculate the estimated tension. Frequencies with a yellow dot mean that they do not follow the integer pattern and are not correct frequencies, and will not be used in any estimation of the tension. The plan red dot means that the frequencies follow the integer pattern, but are not strong enough to use to calculate the tension of the cable. Figure (4.2) shows an example spectra and the spikes with red, green, and yellow dots.

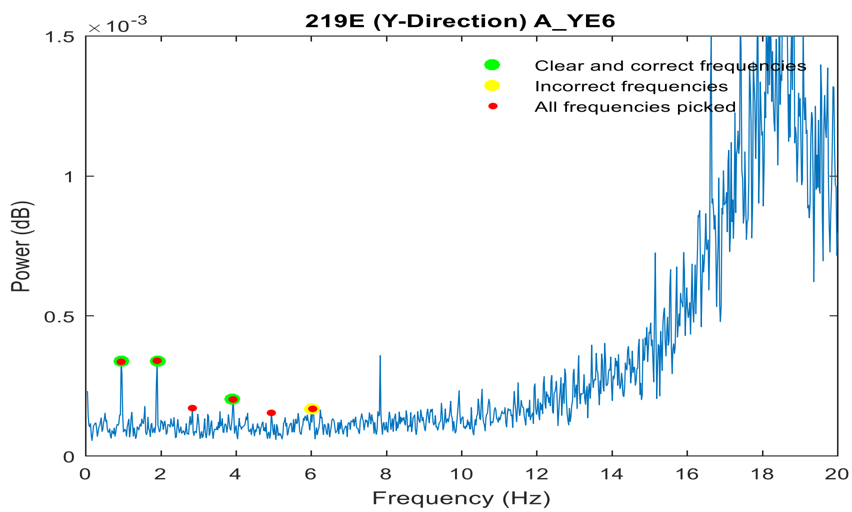

Figure 4.2: The Spikes with Red, Green, And Yellow Dots

By using each of these frequencies with its mode number in Equation (1.1), the tension in the cable can be calculated. Then the average of the cable tension resulting from these frequencies will represent the final tension of the cable. The MATLAB script file is in Appendix (B).

4.3 Wind Event Data Analysis

The data that will be considered for analysis purpose is from Winter Storm Jonas January, 23rd 2016 and Hurricane Matthew, October, 9th 2016.

4.3.1 Data from Winter Storm Jonas, January 2016

Winter Storm Jonas January, 23rd 2016 data were sampled at a rate of 167 samples per second. Data was recorded over a period of several hours and stored in 10-minute records. With this sample rate and recording duration, the data will contain 100,200 points for each sensor. The maximum average wind speed during the day varied from 17.3 to 42.5 mph and the maximum wind gust speed varied from 24.4 to 54.1 mph (Delaware Environmental Observing System). The data was recorded for only nine of the eleven cables due to operational issues with the sensors on stays 319W and 404E. The data that has been analyzed to calculate the frequencies is for a time period with the highest average wind speed for the event: an approximate wind gust of 52.3 mph and an average wind speed of 42.5 mph. The frequencies that were identified from the recorded accelerations are shown in the Table (4.5). The table shows the first six natural frequencies that can be used to estimate the tension in the cables. Some frequencies were not recognized in the spectra and are shown by the empty cells in the table. In Table (4.5), system gauge designation denotes the sensors' direction for that cable name. The frequencies in both directions are almost identical, and the reason is due to the circular shape of the cable (while the accelerations in two directions would not be expected to be the same, the natural frequencies of the circular stay would be the same, regardless of the direction of the recorded data).

Table 4.5: Measured Frequencies (Hz) From Winter Storm Jonas For Wind Gust Speed 52.3 Mph

Stay	System Gauge Designation	Mode number					
		1	2	3	4	5	6
219E	A-YE6	0.938	1.896	--	3.914	--	--
	A-ZE10	0.938	1.896	2.840	3.914	4.788	--
319E	A-YE7	0.971	1.875	2.772	3.731	--	6.462
	A-ZE11	0.971	1.855	2.752	--	--	--
315E	A-YE8	1.060	--	--	--	--	--
	A-ZE12	1.060	2.120	3.201	--	--	--
310E	A-YE9	1.733	3.486	5.198	--	8.684	10.460
	A-ZE13	1.753	3.506	5.219	--	8.684	10.400
310W	A-YW3	1.672	3.364	5.035	7.828	8.480	10.130
	A-ZW5	1.672	3.342	5.035	--	8.480	10.130
305E	A-YE10	2.732	5.484	--	10.950	13.580	--
	A-ZE14	2.732	5.484	7.828	10.950	13.660	--
408E	A-YE12	1.835	3.751	--	7.828	--	11.010
	A-ZE16	1.835	3.731	--	7.828	--	11.050
413E	A-YE13	1.264	2.258	3.792	--	--	--
	A-ZE17	1.264	2.258	3.792	--	--	--
419E	A-YE14	0.979	1.957	2.956	--	--	--
	A-ZE18	0.979	1.957	2.956	3.934	--	5.890

It is clearly shown that in Table (4.5) the “pwelch” command used in the MATLAB script file shows excellent performance for extracting cable natural frequencies during wind events, particularly for high wind speeds, above 40 mph.

An example of the power spectra from the data that were recorded for this specific wind speed is shown in the Figures (4.3) and (4.4). Figures (4.3) and (4.4) show the spectra for the cable 219E in the Y direction and Z direction, respectively. Here again, a red dot denotes a peak that was identified and could potentially be a stay natural frequency, green dots denote ones that have been identified as stay frequencies because they follow the integer ratio criteria of Equation (1.1), and yellow dots do not.

Even though both sensors plotted in the figures are for the same cable, in Figure (4.3), there are three recognizable frequency spikes, while in Figure (4.4) there are five distinct frequency spikes; that is because the data are recorded at the same time for both sensors, so the direction of the wind which will be discussed later has an effect of the frequencies. In Figure (4.3), the signal is influenced by aliasing discussed previously, and this shows up as a wide band of a power starting at approximately 14 Hz. However, this aliasing does not affect identification of the natural frequencies of the cable in the lower frequency range.

From Tables (4.3) and (4.4), it can be seen that the highest theoretical natural frequency is approximately 19 Hz, so frequencies greater than 20 Hz will not be used for analysis purpose, and for this reason the plot is limited to a maximum of 20 Hz. In addition, in this research the frequency exploration is carried out up to the sixth natural frequency ($f6$) that is identified. All other power spectra for other cables and wind speed are found in Appendix (C).

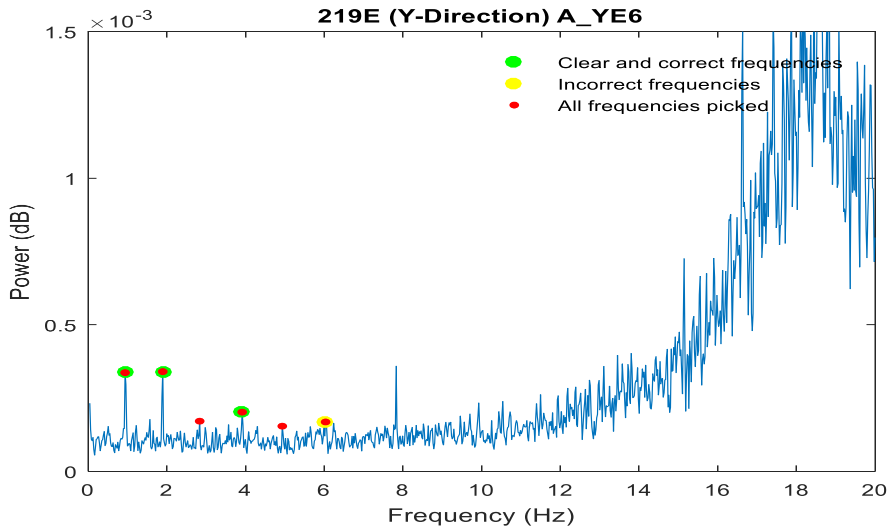

Figure 4.3: Spectra For 219E In the Y Direction (Jan. 2017)

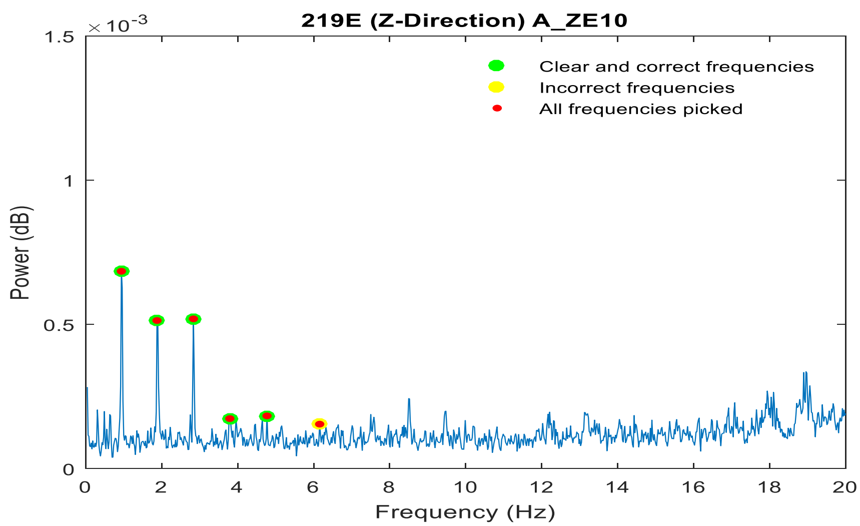

Figure 4.4: Spectra for The Cable 219E In the Z Direction (Jan. 2017)

Table (4.6) shows the mode number for each frequency, which is the ratio of the higher stay frequency divided by the fundamental frequency, which should be close to an integer value if the identified frequencies are stay frequencies. The results show that the frequency rates are all close to an integer value, meaning that the cable frequencies are accurate enough to estimate tension force.

Table 4.6: The Frequency Rate for The Modes

Stay	System Gauge Designation	Frequencies rate for modes				
		2	3	4	5	6
219E	A-YE6	2.02	3.02	4.17	--	--
	A-ZE10	2.02	3.03	--	--	--
319E	A-YE7	1.91	2.83	3.83		
	A-ZE11	1.91	2.83			
315E	A-YE8	--	--	--	--	--
	A-ZE12	2.00	3.02			
310E	A-YE9	2.01	3.00	4.52	5.01	6.04
	A-ZE13	2.00	2.98	4.47	4.95	5.93
310W	A-YW3	2.01	3.01	--	5.07	6.06
	A-ZW5	2.00	3.01	--	5.07	6.06
305E	A-YE10	2.01	--	4.01	4.97	--
	A-ZE14	2.01	2.87	4.01	5.00	--
408E	A-YE12	2.04	--	4.27		6.00
	A-ZE16	2.03	--	4.27	5.02	6.02
413E	A-YE13	1.79	3.00	--	--	--
	A-ZE17	1.79	3.00	--	--	--
419E	A-YE14	2.00	3.02	--	--	--
	A-ZE18	2.00	3.02	4.02	--	6.02

Another example of the power spectra from the data that were recorded for 28.7 mph wind gust and 19.5 mph average wind speed is shown in the Figures (4.5), (4.6), (4.7) and (4.8). The Y and Z direction for the cable 219E are shown in Figures

(4.5) and (4.6), respectively. While Figures (4.7) and (4.8) show the power spectra in Y and Z direction for the cable 315E.

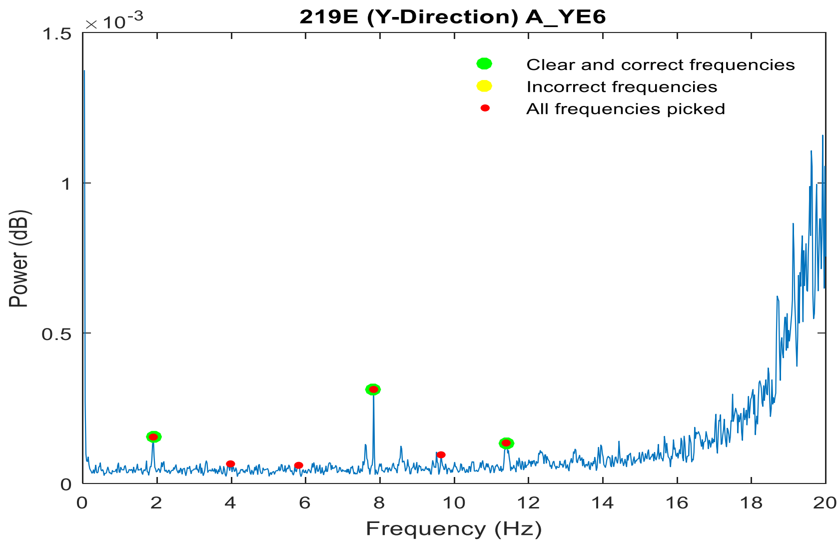

Figure 4.5: The Spectra for the Cable 219E In the Y Direction

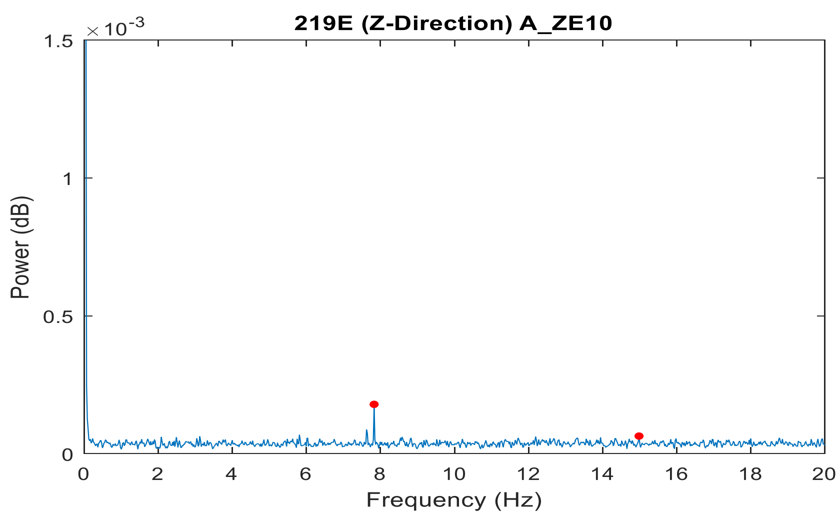

Figure 4.6: The Spectra for The Cable 219E In the Z Direction

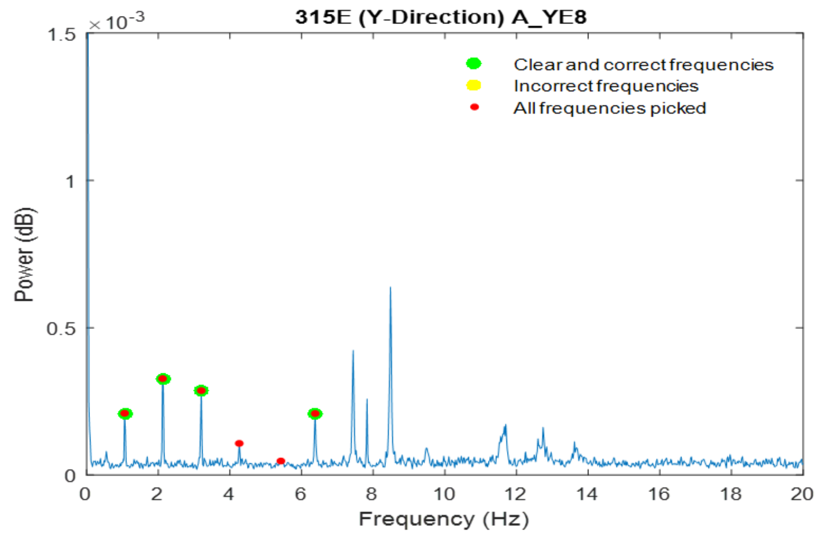

Figure 4.7: The Spectra for The Cable 315E In the Y Direction

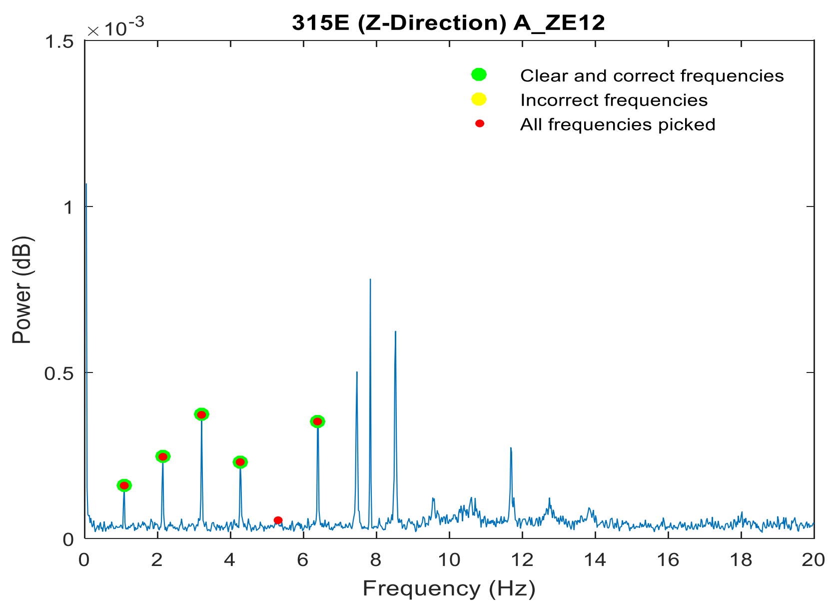

Figure 4.8: The Spectra for The Cable 315E In the Z Direction

In Figures (4.5) and (4.6), the peaks are hard to find at the lower wind speed, however, a few can still be identified. For example, for cable 219E in the Y and Z-directions, there is only one distinct frequency in the Y-direction, and the other distinct frequencies with green dots are higher than mode six. This frequency can be used to estimate the tension in the cable; however, it will not be as accurate as an estimate based on more than one frequency. On the other hand, cable 315E shows four obvious frequencies in the Y-direction and five frequencies in the Z-direction.

Note that there is a well-defined peak at about 7.8 Hz for cables 219E and 315E. Because this frequency shows up in both spectra, which are for stays of different length, and is not close to any theoretical frequency (Table (4.3)), it is assumed that this frequency does not represent any of the natural frequencies of these cables. Theoretically, the motion of the stay can be assumed to be dominated by the stay itself, anchored between two "rigid" points, hence, the sensor measures predominately the vibration of just the stay. However, the stay sensors will also pick up the overall vibration of the bridge. For this reason, there could be other frequencies that show up in the PSD of the cables that are not frequencies of the stay alone but are due to the overall motion of the bridge.

4.3.2 Data from Hurricane Matthew, October 2016

The second acceleration data that are considered for calculating tension force is from Hurricane Matthew on October, 9th 2016. This data was also collected with a sample rate of 167 samples-per-second and for 10-minute periods, for a total of 4 hours and 30 minutes. According to the Delaware Environmental Observing System, the maximum average wind speed and wind gust varied from 15.7 mph to 21.3 mph and from 24 to 31.2 mph, respectively. The wind speed for hurricane Matthew was lower than the maximum wind speed recorded for Winter Storm Jonas. The results of the data analysis suggest that the cables were not excited as much and therefore, fewer frequencies could be identified from the spectra. Table (4.7) shows the estimated natural frequencies of the cables for the higher wind speed during this event, which is 31.2 mph gust and 20 mph on average.

Table 4.7: Estimated Natural Frequencies (Hz) of The Cables from Hurricane Matthew Data for Wind Gust Speed 31.2 Mph

Stay	System Gauge Designation	Mode Number					
		1	2	3	4	5	6
219E	A-YE6	--	2.059	--	--	--	--
	A-ZE10	--	1.896		--	5.341	--
319E	A-YE7	--	1.855	--	--	--	--
	A-ZE11	Not Clear					
319W	A-YW2	--	2.059	--	--	--	--
	A-ZW4	Not Clear					
315E	A-YE8	1.060	2.141	3.201	4.261	--	--
	A-ZE12	not clear					
310E	A-YE9	No Data					
	A-ZE13	1.733	3.486	5.219	--	8.684	--
310W	A-YW3	--	--	--	--	7.828*	--
	A-ZW5	--	--	--	--	7.828*	--
305E	A-YE10	2.732	5.463	8.451	11.399	14.200	--
	A-ZE14	2.732	5.463	8.453	11.399	14.200	--
408E	A-YE12	1.876	--	--	7.828*	--	--
	A-ZE16	--	--	--	7.828*	--	--
413E	A-YE13	--	--	--	--	--	7.624*
	A-ZE17	--	--	--	--	--	7.828*
419E	A-YE14	Not Clear					
	A-ZE18	Not Clear					

*not natural frequency of the cable

Table (4.7) shows the first six frequencies. There were no data recorded for cable 404E. For cables 319E in the Z- direction, 319W in the Z- direction, and 419E in both directions, there were obvious frequencies identified for modes higher than six. Also, there is one common frequency at 7.82 Hz that is identified for most cables. As this frequency has been described before for the data from Winter Storm Jonas it is assumed to be a global frequency of the bridge and it cannot be used to estimate the tension for the cables.

Figures (4.9) and (4.10) show the spectra for cable 219E in both directions. For the Y- direction for cable 219E in Figure (4.9), nothing can be identified with confidence, even though the first frequency was marked as a clear and correct frequency. Using the first frequency to estimate the tension of the cable will generate no confidence that this frequency is the actual frequency of the cable, because there are discernible frequency peaks around it with approximately the same power. However, the wind direction vibrated cable 219E in the Z-direction in a way that makes it possible to distinguish the actual frequency of the cable with more accuracy.

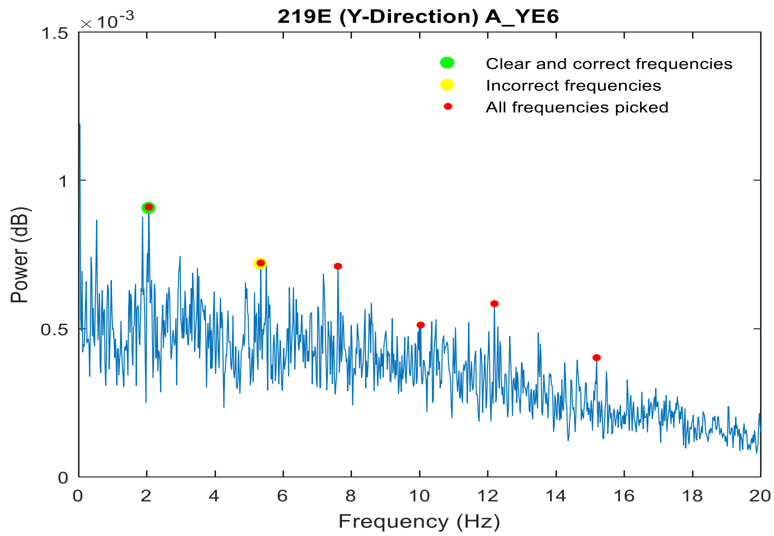

Figure 4.9: The Spectra for The Cable 219E In the Y Direction

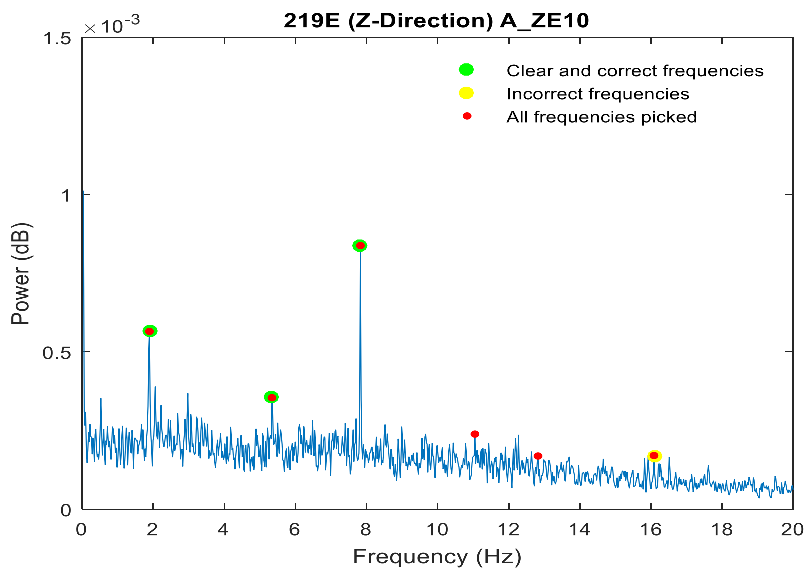

Figure 4.10: The Spectra for The Cable 219E In the Z Direction

Figures (4.11) and (4.12) show another example of spectra for cable 319W. The scale was zoomed in for this figure to show the entire spectra. This cable demonstrates almost the same behavior of cable 219E, but here the Z- direction has no obvious frequencies. The Z- direction sensor is not able to capture the discernible frequency peaks, despite the fact that it has the same properties of cable 219E, with the exception that it is located on the west side of the bridge. Figure (4.12) shows the results for the Z-direction that do not provide any reasonable results for the frequencies.

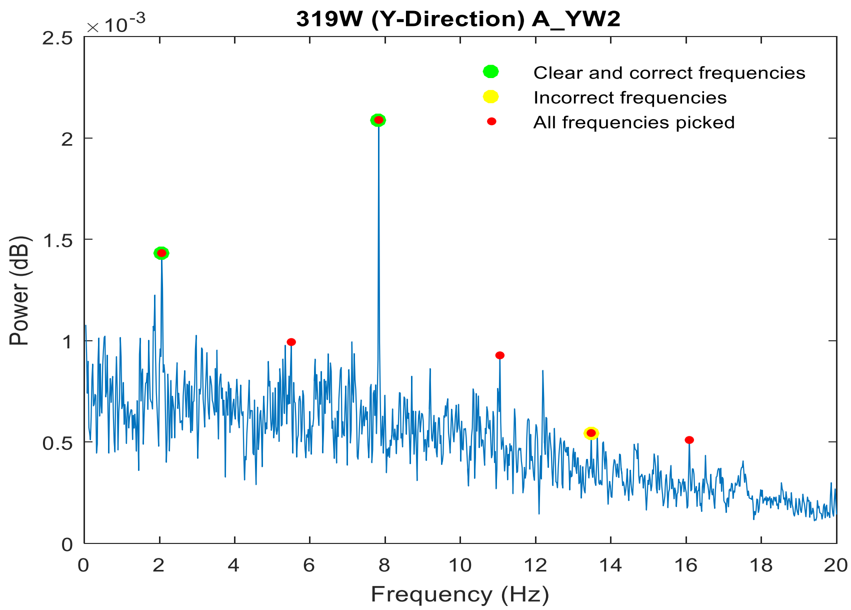

Figure 4.11: The Spectra for The Cable 319W In the Y Direction

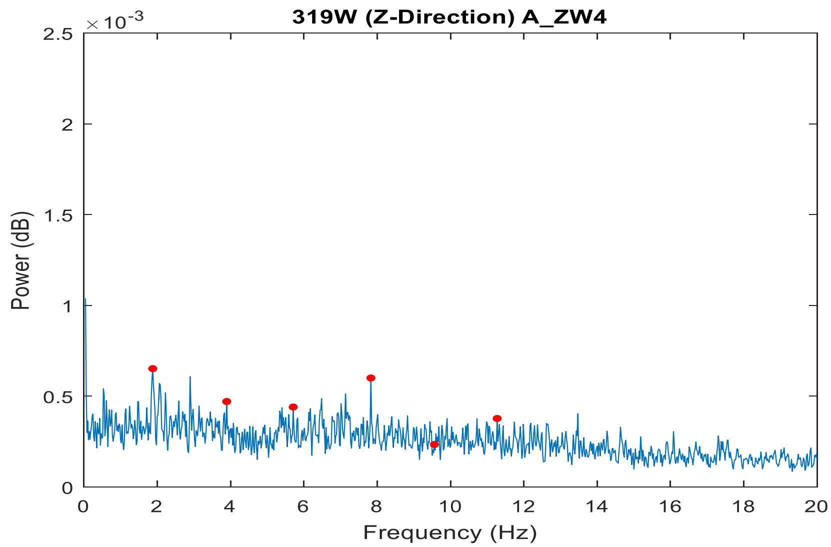

Figure 4.12: The Spectra for The Cable 319W In the Z Direction

The different properties for each cable such as the length and the mass per unit length play an important role in determining the natural frequencies of the cables. In addition, the dampers that are attached to each cable are the most important factors that influence the identification of the natural frequencies. For these reasons, cable 305E in both direction shows obvious frequency peaks that can be used to estimate the stay force. The length of cable 305E is approximately one third the length of cables 219E and 319W. Furthermore, the minimum design damping ratio of cable 305E is almost half the design damping ratio of cables 219E and 319W, meaning that there is a greater chance for cable 305E to vibrate smoothly. Figures (4.13) and (4.14) show the spectra for cable 305E in the Y and Z directions, respectively. The power of the peaks for cable 305 E were small in both directions which required zooming in on the spectra, but the peaks are clearly identified from the PSD.

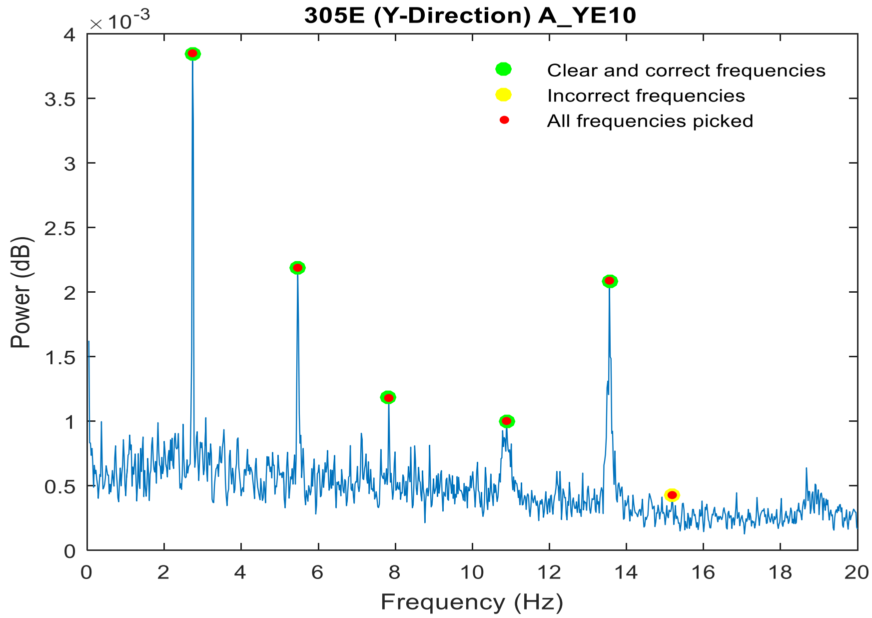

Figure 4.13: The Spectra for The Cable 305E In the Y Direction

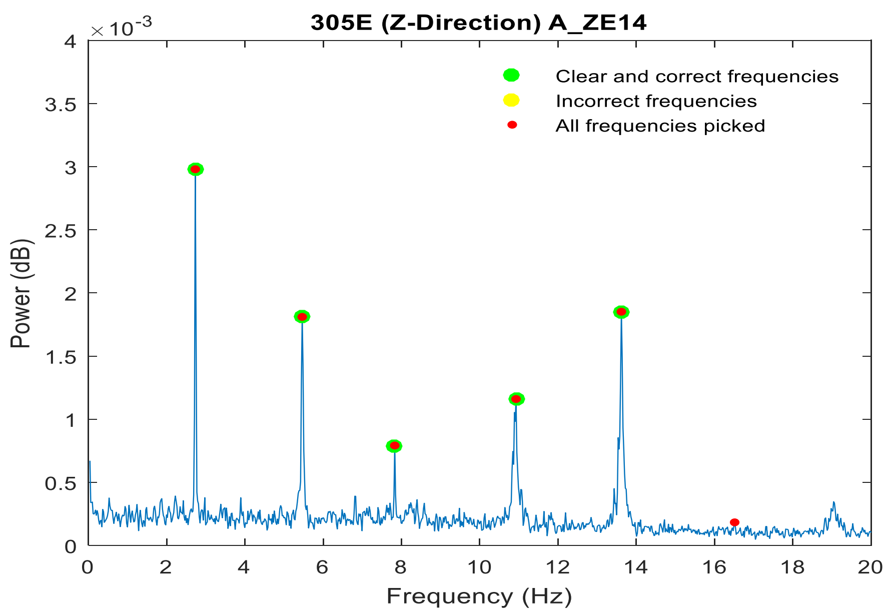

Figure 4.14: The Spectra for The Cable 305E In the Z Direction

4.4 Data Analysis

The frequency and tension comparison for both data from winter storm Jonas and hurricane Matthew with results from the end of construction and the hydraulic jack test will be presented in this section.

4.4.1 Winter Storm Jonas and Hurricane Matthew Data Analysis

The frequencies of the cables presented in Table (4.5) for high wind speed are approximately close to the frequencies from Table (4.3) (the frequencies from the end of construction design tension) with a difference of no more than 0.5 for a few of them. This means that estimated tension for most cables are similar to the tension from the end of construction. Using the frequencies from Table (4.5) and Equation (1.1), the tension force can be calculated from the measured frequencies. Table (4.8) shows the estimated tensions calculated from the frequencies at a wind gust speed of 53 mph.

Table 4.8: Comparison of Tension Force for Wind Gust Speed 52.3 Mph

Stay	System Gauge Designation	Vibration based estimated tension (kips)	Design Tension (kips)	Percent difference (%) ((E-D)/E) *100	End of construction contractor measured tension (kips)	Percent difference (%) ((E-M)/E) *100
219E	A-YE6	1338	1438	-7	1439	-8
	A-ZE10	1330	1438	-8	1439	-8
319E	A-YE7	1297	1432	-10	1386	-7
	A-ZE11	1250	1432	-15	1386	-11
315E	A-YE8	795	768	3	767	4
	A-ZE12	776	768	1	767	1
310E	A-YE9	888	758	15	895	-1
	A-ZE13	884	758	14	895	-1
310W	A-YW3	804	758	6	872	-8
	A-ZW5	819	758	7	872	-6
305E	A-YE10	541	576	-6	578	-7
	A-ZE14	532	576	-8	578	-9
408E	A-YE12	710	688	3	725	-2
	A-ZE16	716	688	4	725	-1
413E	A-YE13	819	934	-14	885	-8
	A-ZE17	818	934	-14	885	-8
419E	A-YE14	1215	1127	7	1225	-1
	A-ZE18	1217	1127	7	1225	-1

The third column in Table (4.8) shows the estimated tension based on the measured vibration during the event, while the forth column shows the design tension. Calculating the percent different between the estimated tension and design tension is presented in the fifth column. The percentage difference ranges from -15% to 14%, where a plus value means that the estimated tension is higher than the design tension and vice versa. In case the estimated tension is less than the design tension strength, there will not be a risk on the bridge, while, there could be a concern about the bridge if the estimated tension from measured vibration is higher than the design tension.

However, the acceleration recorded during very high wind speeds produces no more than a 14% different between the measured tension of the cable and design tension, which is not a high value. However, comparing estimated tension with design tension is not as valuable as doing the comparison with the end of construction measured tension. This is because the last determines the final profile of the bridge and can be considered a more reliable estimate of the actual tension in the stay cables. The last column in Table (4.8) shows the percentage difference between the estimated tension and the measured tension from the end of construction hydraulic jacking. It can be seen that the difference between the estimated and the end of construction tension is in many cases less than the difference relative to the design tension, and all the values are negative except for cable 315E which was positive and can be considered a negligible difference. The chart in Figure (4.15) shows another comparison of the results between the estimated tension from measured vibration at 52.3 mph and the end of construction tension.

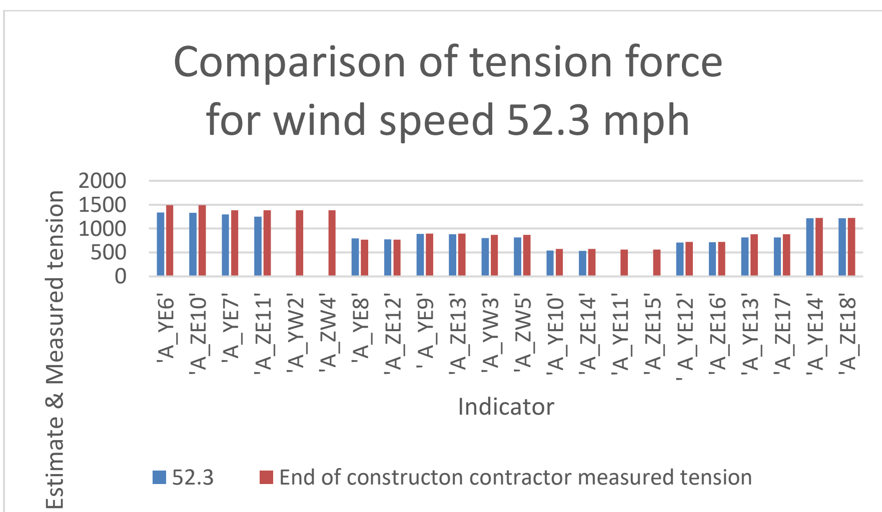

Figure 4.15: Comparison of Estimated Tension from Measured Vibration At 52.3 Mph and The End of Construction Tension

The hope is that the high wind speed does not induce additional tension into the cables, which might cause some concern about the safety of the bridge, in case this tension exceeds the design tension or even the end of construction tension. From this analysis, it is obvious the high wind speed has no influence on the performance of the cables, especially this very high wind speed of 52.3 mph.

Table (4.9) shows the average estimated tension for all of the stays from Winter Storm Jonas for different wind speeds and directions (0 degree means that the wind direction is approximately parallel to the deck, and it is north).

Table 4.9: Estimated Tension for Different Wind Speeds

Stay	System Gauge Designation	Vibration based estimated tension for Wind gust (mph) Wind Speed Average (mph) Direction (°)									End of constructon contractor measured tension
		52.3	50.6	49.8	49.2	48.7	46.7	32.3	30.6	28.7	
		42.5	41.8	39.5	38.9	37.6	33.8	25	22.2	19.5	
		55.3(NE)	39.7(NE)	30.4(NNE)	36.4(NE)	29.5(NNE)	25.2(NNE)	13.3(NNE)	8.8(N)	358.8(N)	
219E	A-YE6	1338	1333	1382	1411	1392	1382	1350	1394	1394	1493
	A-ZE10	1330	1346	--	1349	1346	1346	--		1394	1493
319E	A-YE7	1297	1288	1281	1282	--	not clear	1110	--	1101	1386
	A-ZE11	1250	1266	1285	1280	--	1293	1288	1290	1264	1386
315E	A-YE8	795*	752	752	752	752	755	758	758	756	767
	A-ZE12	776*	696	760	752	759	755	759	761	777*	767
310E	A-YE9	888	888	888	882	888	881	882	882	882	895
	A-ZE13	884	884	881	881	885	881	882	881	882	895
310W	A-YW3	804	819	823	821	829	800	825	807	810	872
	A-ZW5	819	823	823	825	823	828	830	829	827	872
305E	A-YE10	541	539	541	545	542	534	530	530	532	578
	A-ZE14	532	534	532	534	545	542	541	542	543	578
408E	A-YE12	710	704	704	697	702	702	755*	679*	717	725
	A-ZE16	716	673	698	655	676	690	--			725
413E	A-YE13	819	819	819	819	819	823	805	805	--	885
	A-ZE17	818	821	819	821	821	821	--		836	885
419E	A-YE14	1215	1224	1222	1241	1218	1210	1235*	1235*	--	1225
	A-ZE18	1217	1227	1241	1227*	1224	1224	--			1225

* estimated tensions for cables are higher than their end of construction design tension

The table compares the tension during different wind speeds and with end of construction contractor measured tension. Each column in Table (4.9) represents the average estimated tension during specific wind gust speeds and directions that are listed in the headings of each column. The comparison of estimated tensions from the wind events to the end of construction loads shows that all the estimated tensions for the cables are below the end of construction design tension, except for some cables that are higher than their end of construction design tension. These are shown with an asterisk in Table (4.9). However, the percent differences are very small, no more than 15%.

The average estimated tensions from Hurricane Matthew data are presented in Table (4.10). This wind event was quite steady, more so than in the Winter Storm Jonas event, which can provide another check for cables behavior under this type of wind. The empty cells in the table mean there were no obvious frequencies, or the identification was deemed poor, to use in estimating the tension force. The comparison of estimated tensions from these wind events to the end of construction tensions shows that all the estimated tensions for the cables are below the end of construction design tension.

Table 4.10: Average Estimated Tensions from Hurricane Matthew Data

Stay	System Gauge Designation	Vibration based estimated tension for Wind gust (mph) Wind Speed Average (mph) Direction (°)		
		31.2 20.0 356.3(N)	30.5 20.1 356.4(N)	24.0 15.7 0.2(N)
219E	A-YE6	--	--	--
	A-ZE10	1270	--	--
319E	A-YE7	1269	--	--
	A-ZE11	1321	1292	
319W	A-YW2	--	--	--
	A-ZW4	1321	--	--
315E	A-YE8	795	795	760
	A-ZE12	--	--	--
310E	A-YE9	--	--	--
	A-ZE13	881	878	877
310W	A-YW3	--	815	--
	A-ZW5	--	815	815
305E	A-YE10	539	530	529
	A-ZE14	539	529	529
408E	A-YE12	694	--	--
	A-ZE16	--	--	--
413E	A-YE13	--	825	825
	A-ZE17	--	--	818
419E	A-YE14	--	--	--
	A-ZE18	--	--	--

4.5 Root Mean Squared of Measured Acceleration

The Root Mean Square (RMS) of the measured stay acceleration is another measure of the “strength” of the signal, i.e., the magnitude of the stay vibration. RMS is calculated as:

$$E_{RMS} = \sqrt{\frac{x_0^2+x_1^2+\cdots+x_{N-1}^2}{N}} \qquad (4.1)$$

where E_{RMS} is the root mean squared of the signal, N is total number of samples, and $(x_0, x_1, \cdots, x_{N-1})$ are the discrete sampled values.

Figures (4.16) is an example of raw time history acceleration data for cable 219E in the Y-direction, for various wind speeds and directions. Figure (4.16) shows the effect of the wind speed and direction on recording acceleration data. It can be seen from the figure that the amplitudes of the acceleration are large for the high wind speed such as 52.1 and 50.6 mph, and become less and less with decreasing the wind speed. Although the change in the amplitude for the acceleration is not obvious enough for the wind speed less than 48 mph, the RMS in the following figures describe the influence of the speed in a more obvious way, which is one advantage of calculating RMS for the signal.

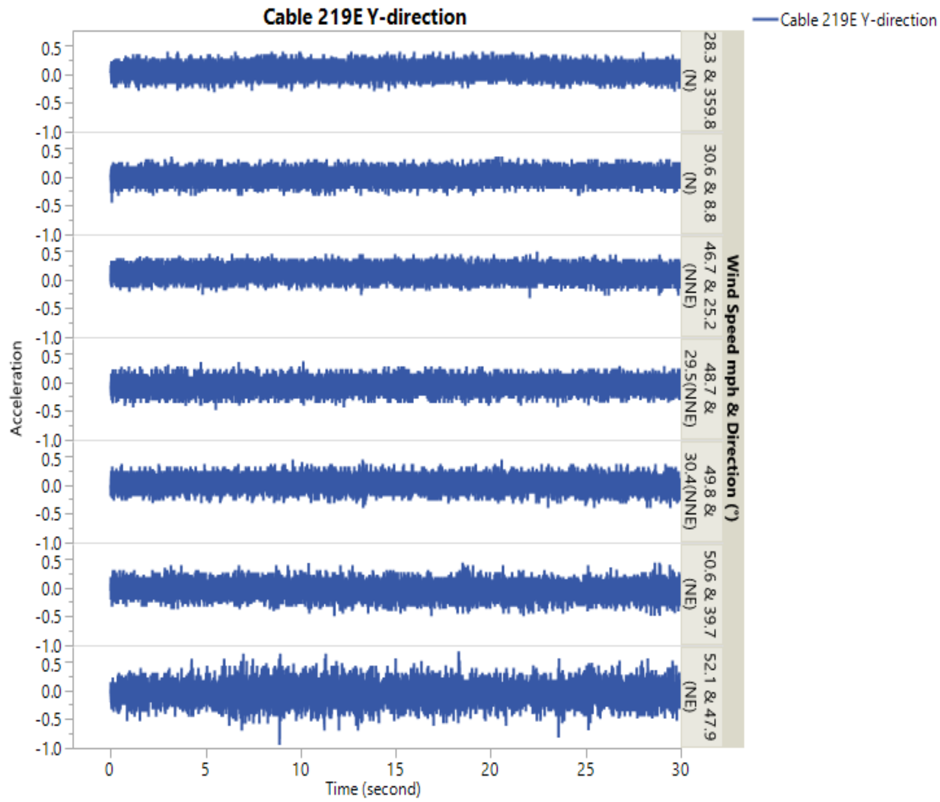

Figure 4.16: Time History Domain for Different Wind Speed for Cable 219E Y-Direction

RMS for different wind speeds from Winter Storm Jonas for cables 219E and 305E can be seen in Figures (4.17) and (4.16). 219E is the longest cable, and 305E is one of the shorter cable that has been monitored. Cable 404E might be better to use here, because it is the shortest cable, but there is no data for this stay. Thus, 219E and 305E provide a good representation of the behavior of the other cables.

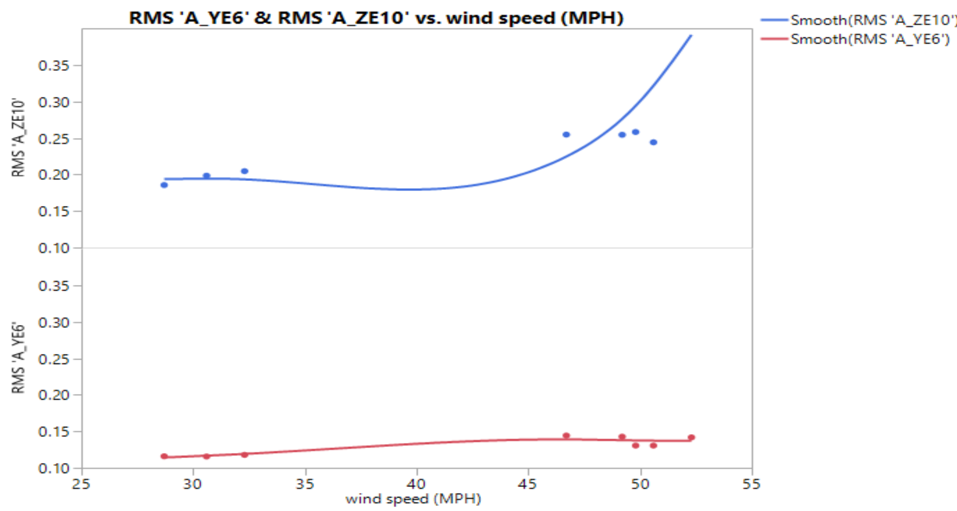

Figure 4.17: The RMS For Cable 219E (Y & Z Direction) Using Smooth Line

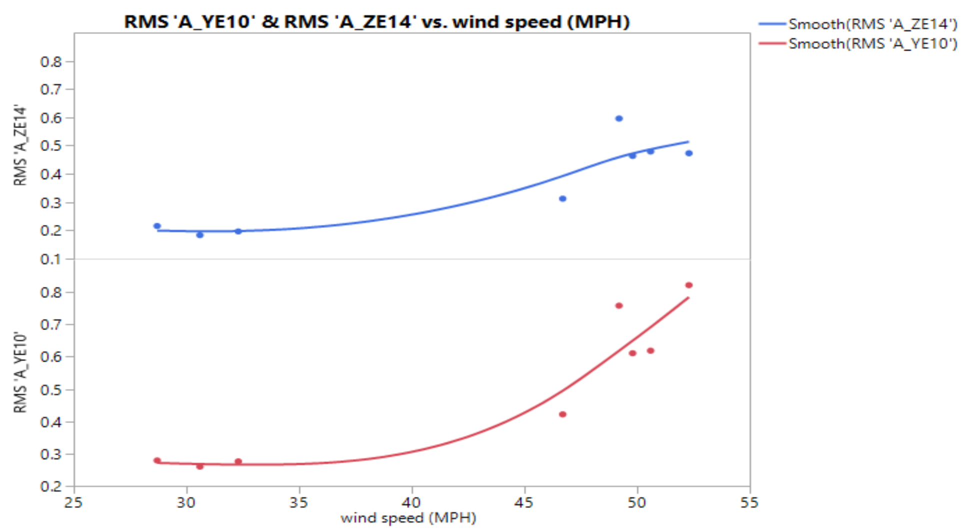

Figure 4.18: The RMS For Cable 305E (Y & Z Direction) Using Smooth Line

There is a general trend that with increasing wind speed there is an increase in the RMS of the signal. It is important to notice that in Figure (4.17) the RMS for the Y- direction (the graph on the bottom of the figure) is much less than the RMS for the Z- direction. The reason is because of the effect of wind direction and the fact that both direction Y and Z have a different plane to vibrate in as discussed in Chapter 3. This will be discussed in more detail in the next section.

Another way to measure a recorded signal's strength is to calculate the maximum or the absolute peak magnitude in the acceleration data. Figures (4.19) and (4.20) show the absolute peak value in the signal for the cables 219E and 305E using the same data that has been used to calculate the RMS.

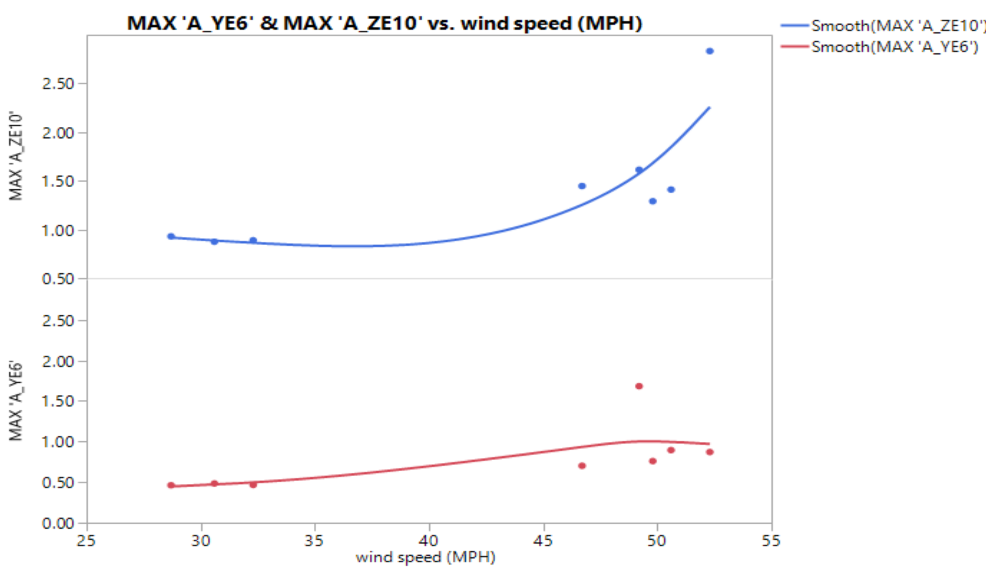

Figure 4.19: The Absolute Peak Value for Cable 219E (Y & Z Direction) Using Smooth Line

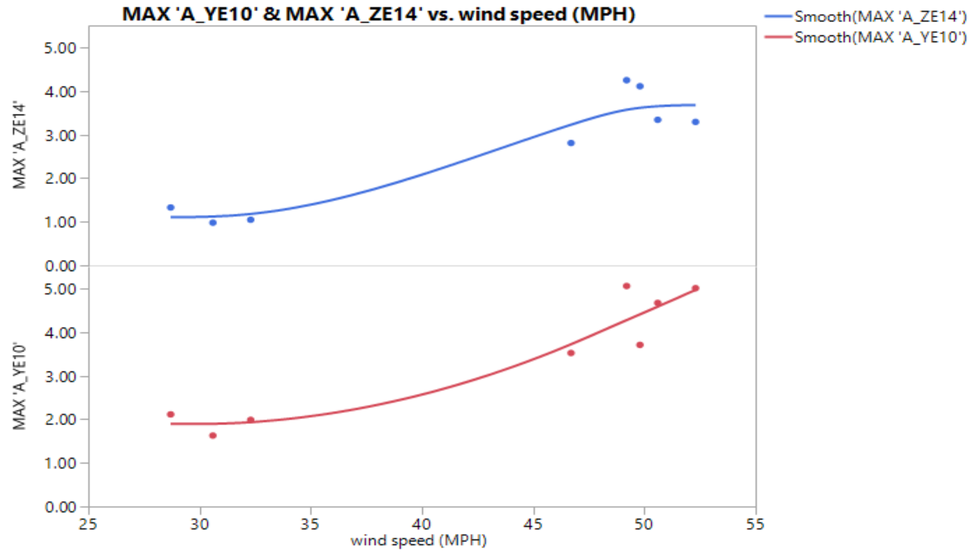

Figure 4.20: The Absolute Peak Value for Cable 305E (Y & Z Direction) Using Smooth Line

From the above figures, it can be seen that the majority of the large amplitude responses occur between 40 and 55 mph wind speed. Table (4.11) shows the RMS and the maximum amplitude for the cables during Winter Storm Jonas for different wind speeds.

Table 4.11: RMS And the Max Amplitude of The Winter Storm Jonas Time History

Stay	System Gauge Designation	RMS for wind gust 52.3	Max Abs value	RMS for wind gust 50.6	Max Abs value	RMS for wind gust 49.8	Max Abs value	RMS for wind gust 49.2	Max Abs value	RMS for wind gust 46.7	Max Abs value	RMS for wind gust 32.3	Max Abs value	RMS for wind gust 30.6	Max Abs value	RMS for wind gust 28.7	Max Abs value
219E	A-YE6	0.14	0.87	0.13	0.90	0.13	0.76	0.14	1.68	0.14	0.70	0.12	0.47	0.12	0.49	0.12	0.46
	A-ZE10	0.49	2.83	0.24	1.41	0.26	1.29	0.25	1.62	0.25	1.45	0.20	0.89	0.20	0.88	0.19	0.93
319E	A-YE7	0.50	3.18	0.56	3.17	0.47	2.33	0.63	3.16	0.43	3.27	0.17	0.87	0.17	0.90	0.17	1.95
	A-ZE11	0.50	2.96	0.53	3.64	0.46	2.46	0.60	3.75	0.43	2.54	0.22	1.50	0.19	1.57	0.18	2.46
315E	A-YE8	0.72	5.51	NaN	5.60	0.59	4.69	0.78	4.90	0.45	3.28	0.19	0.90	0.18	0.91	0.15	0.70
	A-ZE12	0.62	3.97	0.67	3.58	0.64	3.16	0.73	3.81	0.53	3.14	0.18	0.80	0.16	0.74	0.14	0.68
310E	A-YE9	0.21	1.23	0.19	1.16	0.22	1.19	0.21	1.21	0.25	1.30	0.22	1.40	0.19	0.93	0.14	0.87
	A-ZE13	0.17	1.19	0.13	0.69	0.15	0.79	0.15	0.73	0.16	0.78	0.14	0.66	0.13	0.55	0.12	0.56
310W	A-YW3	0.29	1.97	0.21	1.32	0.22	1.43	0.23	1.44	0.19	1.13	0.15	0.74	0.15	0.62	0.15	0.75
	A-ZW5	0.22	1.59	0.16	0.97	0.18	1.05	0.18	1.05	0.17	1.11	0.14	0.65	0.15	0.60	0.16	0.74
305E	A-YE10	0.82	5.01	0.62	4.67	0.61	3.71	0.76	5.06	0.42	3.52	0.28	1.99	0.26	1.63	0.28	2.11
	A-ZE14	0.47	3.29	0.48	3.34	0.46	4.11	0.60	4.25	0.31	2.81	0.20	1.05	0.18	0.98	0.22	1.33
408E	A-YE12	0.47	3.17	0.24	1.57	0.27	1.55	0.29	1.76	0.23	1.44	0.19	1.10	0.18	1.01	0.19	1.28
	A-ZE16	0.43	2.37	0.26	1.38	0.26	1.39	0.29	1.66	0.24	1.25	0.21	0.96	0.20	0.96	0.20	0.89
413E	A-YE13	0.32	1.66	0.19	1.39	0.22	1.05	0.24	1.45	0.20	1.19	0.16	0.73	0.15	0.67	0.17	0.98
	A-ZE17	0.26	1.37	0.18	1.13	0.20	0.99	0.23	1.33	0.18	0.98	0.16	0.75	0.16	0.74	0.18	0.96
419E	A-YE14	0.22	1.19	0.16	0.89	0.20	0.96	0.20	1.19	0.18	0.98	0.16	0.78	0.16	0.75	0.19	0.85
	A-ZE18	0.25	1.64	0.16	1.03	0.18	0.80	0.20	1.02	0.16	0.67	0.13	0.59	0.14	0.62	0.14	0.71

4.6 Effect of the Speed and Direction of the Wind

Because of the slenderness of the cables, wobble, low lateral rigidity and low damping ratio, the cables are highly exposed to the influence of the wind, whether the speed or direction. Hence, environmental forces such as wind speed can easily put cable-stayed bridges under the risk of exciting into enormous motion. Because the cable connects all the bridge structures together, the influence of the wind on the bridge can be represented as oscillations of the cable (Larsen & Larose, 2015). Also, when the bridge's deck is excited by winds, that will lead to even so low amplitude oscillations on the cables at "a frequency corresponding to a harmonic of the eigenfrequency of the mode of the deck that is excited" (Larsen & Larose, 2015). That is what can be seen in the Indian River Inlet bridge with the frequency 7.8 Hz for all cables. Larsen & Larose add that using dampers on the cables might affect the dynamic motion of the deck or the pylon. For example, if the damper on the cable "is negative", that will cause vibration for both cable stays and deck at the same frequencies. Because the wind load is a dynamic load that varies in magnitude, steadiness, and direction, the oscillation of bridge subjected to wind load will be different also. From that the importance of studying the influence of the wind speed on the entire structure of the bridge can be concluded.

Figure (4.21) shows the power spectra for Cable (219E) Y- direction for different wind speeds during Winter Storm Jonas event. The directions of the Winter Storm Jonas wind data either come from the north or north-east directions, so the wind direction varied somewhat during the event. There is some change in the characteristics of the spectra with increasing wind speed: certain peaks appear and become more obvious with increasing wind speed, and the number of notable peaks increases with increasing wind speed. However, for low wind speed such as 32.3 mph and lower, there is only one recognizable frequency. It would be acceptable to use this single frequency to estimate the tension in the cable, but may not be as accurate or reliable as an estimate that is based on multiple frequencies. It also can be noticed that the peak at 7.8 Hz is present in all of the spectra, regardless of wind speed.

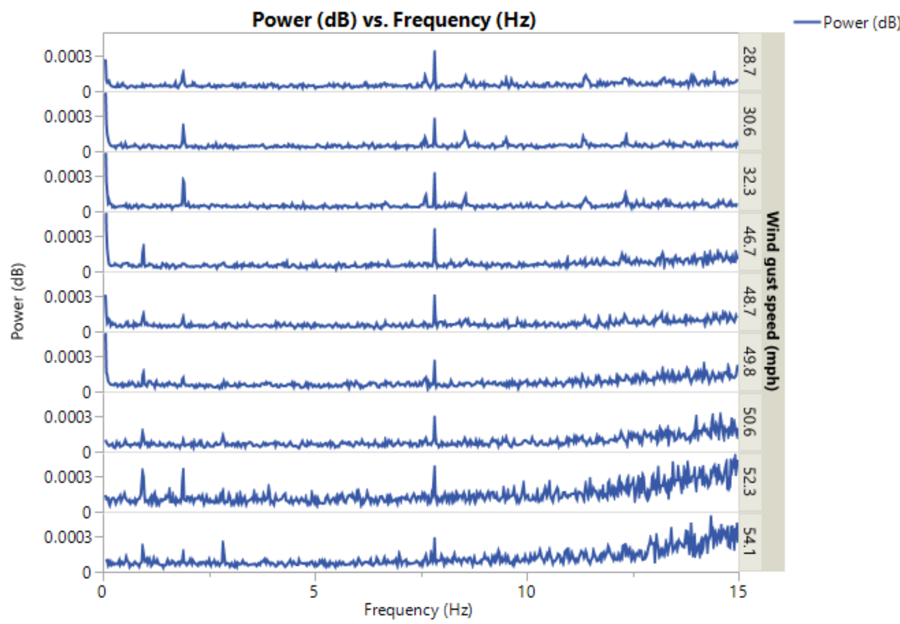

Figure 4.21: Power Spectra for Cable (219E) A_YE6 For Different Wind Speeds

Figure (4.22) shows the comparison of the power spectra for cable 219E in the Z direction for different wind speeds. Figure (4.21) and (4.22) indicate that the strongest frequency responses occurred in the lower modes such as mode 1, 2 and 3. For high wind speeds, almost mode 1 and 2 are the dominant modes, while for lower wind speeds, mode 2 is the dominant mode.

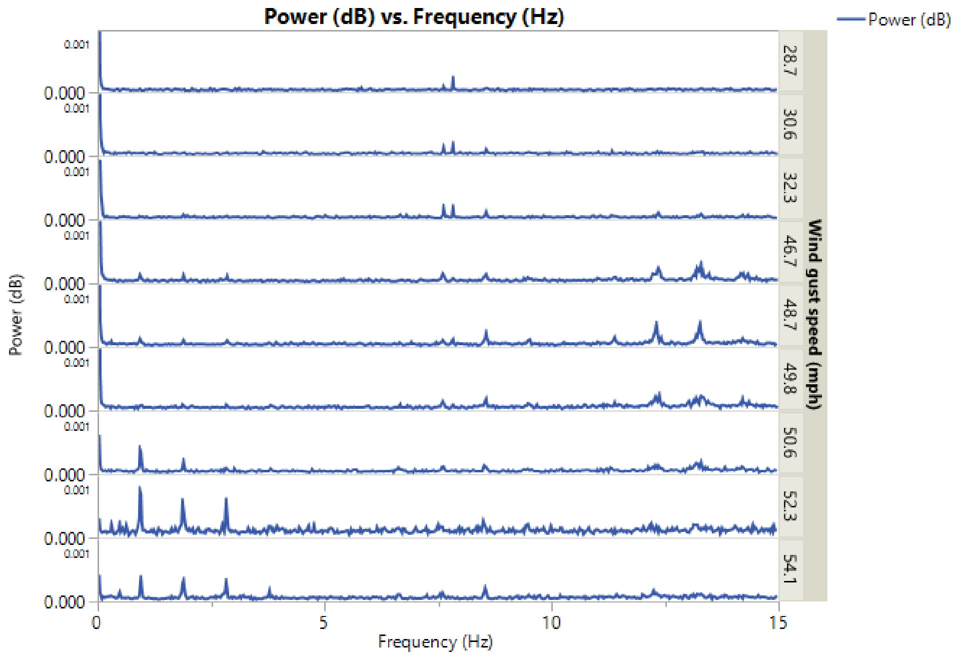

Figure 4.22: Power Spectra for Cable (219E) A_ZE10 For Different Wind Speeds

To examine the consequence of the wind speed and direction in more details, Figures (4.23) and (4.24) show the power spectra for cable 315E in the Y and Z directions, respectively. The data was captured during Hurricane Matthew at a wind speed of 31.2 mph and direction 356.3°(N).

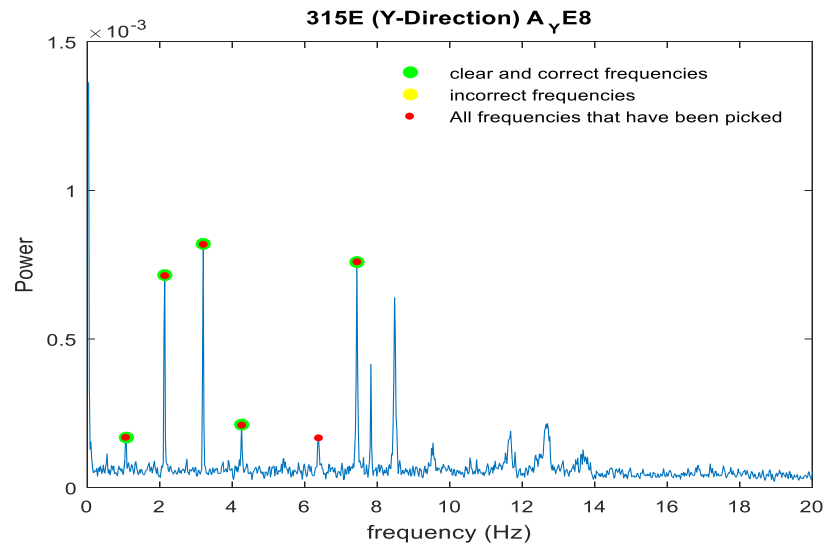

Figure 4.23: The Power Spectra for Cable 315E Y-Direction

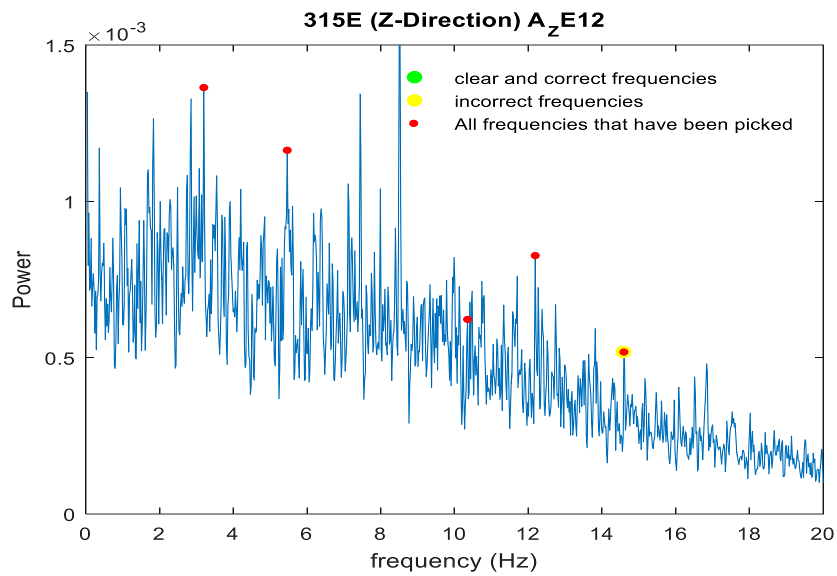

Figure 4.24: The Power Spectra for Cable 315E Z-Direction

The figures give insight into the fact that the frequencies in the Y- direction had more obvious peaks, while in the Z direction, there were no distinguishable frequency peaks. However, this behavior is similar to the behavior of the cable under the effect of the wind direction in Figures (4.21) and (4.22) for wind speed 32.3, 30.6, and 28.7 mph with direction of the wind for all of them toward the north. The two cables show similar behavior regardless of the cables properties such as the length, the mass per unit length, and the damping ratio.

The results presented demonstrate that for many of the stay cables frequencies can be identified with confidence, for a range of wind speeds between 24 and 55 mph. However, for some, there were no obvious identifiable frequencies at wind gusts of 24 mph. That is most likely because of the length of the cables: a long cable is difficult to vibrate under low wind speed. The average wind speed for the data analyzed here ranged from 15.7 to 42.5 mph. For this it can be concluded that there is no certain characteristics required to estimate tension in the stay cables of the Indian River Inlet bridge using taut cable theory, at least for average or gust wind speeds greater than 25 mph and less than 55 mph.

The direction of the wind of the two events studied was from the north or the north-east. With the limited range of directions that was studied, there is not enough information to determine the ideal wind direction for estimating tensions. However, based on the analysis presented here, winds from the north or north-east directions do seem to provide good data for estimating the tension in the stay cables.

Chapter 5

CONCLUSION, DISCUSSION, AND SUGGESTION FOR FUTURE RESEARCH

5.1 Summary

The objective of this research is to develop a quick, automated procedure for estimating the tension in the stay cables on the Indian River Inlet Bridge using acceleration measurements of the stays during moderate to high wind events. In addition, to assess under what wind conditions (i.e., wind speed and direction), the estimates of cable force can be reliably determined.

This study shows that the fiber optic accelerometer sensors used on the stay cables are appropriate and capable of recording acceleration data for the cables when they vibrate enough under the effect of external excitation. In addition, due to the features of the optical fiber sensors such as their small size, light weight, and ease of use, the optical fiber sensors can be considered as an effective and fast tool for the monitoring the tension in the cables.

A literature review was conducted to show that taut cable Equation (1.1) was found to be accurate enough to estimate the tension in "thin" cables. The applicability of this theory has been supported by many previous studies. The reliability of the taut cable theory to estimate accurate tension was validated by comparing the cable tension recorded by the hydraulic jack during the construction and the tension estimated from frequencies from the acceleration data, where the difference between the two tensions was not vast, less than 15%.

Since the data acquisition system that connects to the fiber optic accelerometer sensor provides a large amount of data, a program was developed in MATLAB to process the data. This was found to be an effective and fast method for analyzing the acceleration data. By converting the time domain acceleration data to the frequency domain, by using the "pwelch" command in MATLAB, it was possible to extract and find the natural frequencies of the stay cables. Analysis of data collected during two wind events was presented in chapter 4. This chapter shows the behavior of the bridge and the tension of the cables under different wind speeds.

An investigation was conducted to determine the approximate natural frequencies of the mounted sensors on the stays. It showed that the natural frequencies of the sensors range from 714 to 771 Hz. In addition, to minimize the impact of aliasing, a sample rate of 167 samples-per-second was found to be optimal for measuring the stay vibrations.

5.2 Conclusions

The estimated tension force under high wind speeds (52.3 mph) was presented in table 4.8. Tensions for the cables range from 532 to 1338 kips during Winter Storm Jonas January 2016, while the tension at the end of construction as measured by the contractor ranged from 587 to 1439 kips. The largest difference in tension was -11% in cable 319E (Z-direction), compared with the tension at the end of construction. This difference was negative, meaning that the frequency-based estimate was lower than the contractor measured tension. The largest positive difference in percent was 4% for cable 315E (Y-direction). The estimated tension for different wind speeds and different times for Winter Storm Jonas was presented in Table (4.9). Some stays yielded very consistent estimates, such as stays 310E and 413E, while others showed considerable variability, such as stays 219E and 319E. The maximum tension force for each cable was different under different wind speeds. For example, the maximum tension force for cable 219E was 1394 kips, which resulted from the wind gust of 28.7

mph, while for cable 319E the maximum tension force was 1297 kips, which resulted from the wind gust of 52.3 mph. There is no obvious trend for the tension force under the different wind speeds. However, all the estimated tensions were approximately within the ultimate maximum and minimum ranges from the construction requirements with positive differences of no more than 4%.

The data for the estimated tensions from Hurricane Matthew were presented in Table (4.10). Because of the lower wind speed it was more difficult to identify some of the stay cable frequencies with confidence, and therefore there were fewer estimates of tension from that event. For those that could be identified, the cable tension followed the same trend as the tension from the Winter Storm Jonas: all of the cable tensions were below the tension measured by contractor at the end of construction.

The RMS result of the accelerations data showed an approximate linear relationship between the acceleration of the cable and the wind speed. Even though the maximum values of the RMS were from the maximum wind speed, the cables' tension provides evidence that increasing the size of the acceleration data would not affect the tension of the bridge's cable.

For average or gust wind speeds between 25 mph and 55 mph, the tension in the stay cables can be estimated using taut cable theory. In addition, wind directions from north or north-east provide acceptable data for estimating the tension in the stay cables. There is not enough information to determine the validity of other directions to estimate tension for cables.

5.3 Recommendation for Future Research

Based on this research, it is important to take advantage of high wind events to record data and use it for analysis purposes as it can provide clear frequencies that can be used to estimate cable tensions. Also, digital cameras such as virtual visual sensor (VVS) can be used to compute the PSD through which the fundamental frequency of the vibration of structural systems can be computed and measured. This new technology does not require cabling and is easy to install. Also, by using spline fitting of VVS the modal shapes can be reconstructed in the time domain. Moreover, the spatial and mass constraints cannot affect VVS due to its features such as its non-invasive and highly portable nature (Song at al, 2014).

REFERENCES

Bracewell, R. N., & Bracewell, R. N. (1986). *The Fourier transform and its applications* (Vol. 31999). New York: McGraw-Hill.

Barnhart, N., Halvarsson, P., & Butler K. V. (April 2012). The first to last. (Indian River Inlet Bridge in Delaware). *Civil Engineering American Society of Civil Engineers v82 (n4):* 48-55.

Cho, S., Lynch, J. P., Lee, J. J., & Yun, C. B. (2009). Development of an automated wireless tension force estimation system for cable-stayed bridges. *Journal of Intelligent Material Systems and Structures*.

Cho, S., Lynch, J. P., Lee, J. J., & Yun, C. B. (2010). Development of an automated wireless tension force estimation system for cable-stayed bridges. *Journal of Intelligent Material Systems and Structures*, *21*(3), 361-376.

Choudhury, J. R., & Hasnat, A (August 2015). Bridge collapses around the world: Causes and mechanisms.

Irvine, H. M., & Caughey, T. K. (1974, December). The linear theory of free vibrations of a suspended cable. In *Proceedings of the Royal Society of London A: Mathematical, Physical and Engineering Sciences* (Vol. 341, No. 1626, pp. 299-315). The Royal Society.

Irvine, H. M., & Griffin, J. H. (1976). On the dynamic response of a suspended cable. *Earthquake Engineering & Structural Dynamics*, *4*(4), 389-402.

Kim, B. H., & Park, T. (2007). Estimation of cable tension force using the frequency-based system identification method. *Journal of Sound and Vibration*, *304*(3), 660-676.

Larsen, A., & Larose, G. L. (2015). Dynamic wind effects on suspension and cable-stayed bridges. *Journal of Sound and Vibration*, *334*, 2-28.

National Instruments. (2006). "Aliasing and Sampling at Frequencies Above the Nyquist Frequency ." http://www.ni.com/white-paper/300

Nugroho, G., Priyosulistyo, H., & Suhendro, B. (2014). Evaluation of Tension Force Using Vibration Technique Related to String and Beam Theory to Ratio of Moment of Inertia to Span. Procedia Engineering, *95*, 225-231.

Rogers, M. J., Alexander, J. I. D., & Snyder, R. S. (1990). Analysis techniques for residual acceleration data.

Rogers, M. J., Hrovat, K., McPherson, K., Moskowitz, M. E., & Reckart, T. (1997). Accelerometer data analysis and presentation techniques.

Rawat, Tarun Kumar. (2015). Digital Signal Processing. Oxford University Press.

Starossek, U. (1994). Cable dynamics-a review. *Structural Engineering International*, *4*(3), 171-176.

Song, Y. Z., Bowen, C. R., Kim, A. H., Nassehi, A., Padget, J., & Gathercole, N. (2014). Virtual visual sensors and their application in structural health monitoring. *Structural Health Monitoring*, *13*(3), 251-264.

Triantafyllou, M. S., & Grinfogel, L. (1986). Natural frequencies and modes of inclined cables. *Journal of Structural Engineering*, *112*(1), 139-148.

Thusu, R. (2011). Medical sensors facilitate health monitoring. *Frost & Sullivansensors, 1st April. Available At:*Http://Www. *Sensorsmag. Com/Specialty-Markets/Medical/Sensors-Facilitate-Health-Monitoring-8365*.

Wardhana, K., & Hadipriono, F. C. (2003). Analysis of recent bridge failures in the United States. *Journal of performance of constructed facilities*, *17*

Zui, H., Shinke, T., & Namita, Y. (1996). Practical formulas for estimation of cable tension by vibration method. *Journal of structural engineering*, *122*(6), 651-656.

Appendix A

THE POWER SPECTRUM FOR THE SENSORS OF THE HURRICANE ARTHUR ON JULY 4th, 2014 DATA

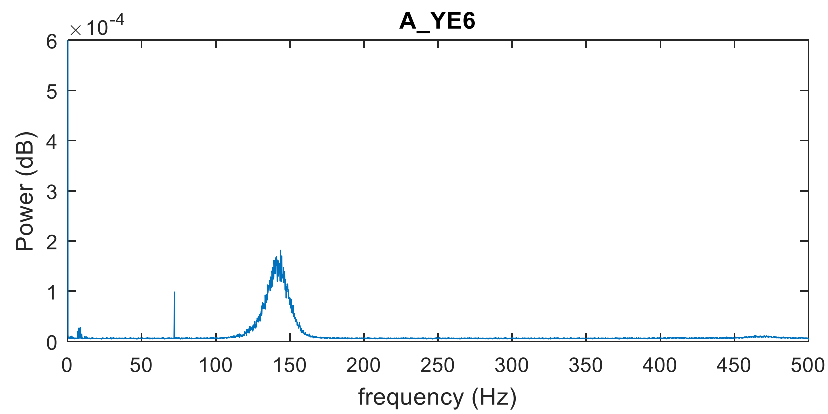

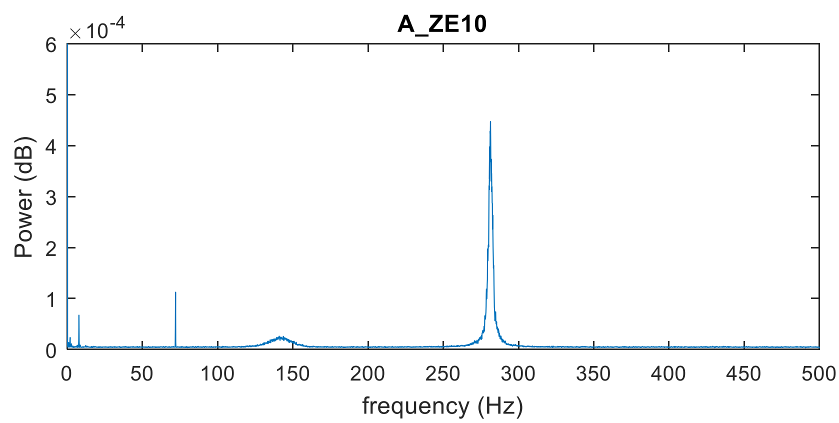

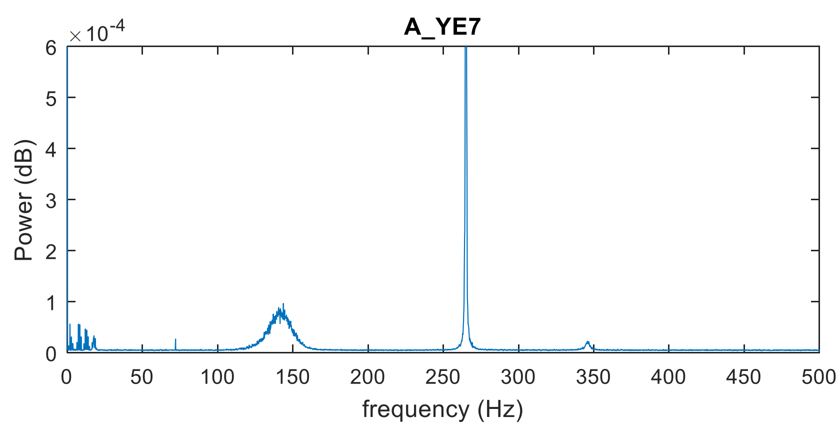

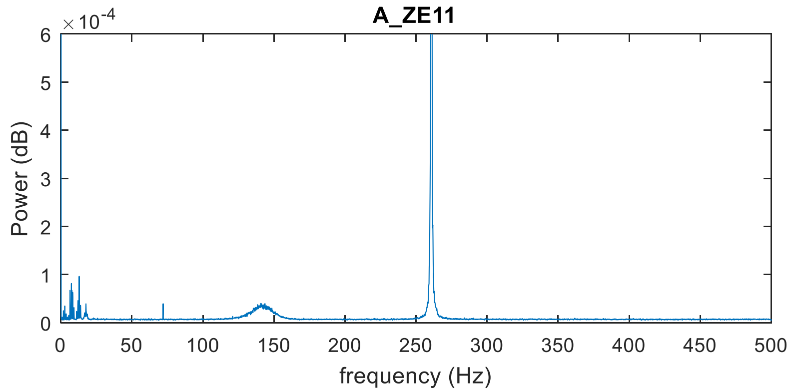
A_ZE11
× 10^-4
Power (dB)
frequency (Hz)
0
50
100
150
200
250
300
350
400
450
500
0
1
2
3
4
5
6

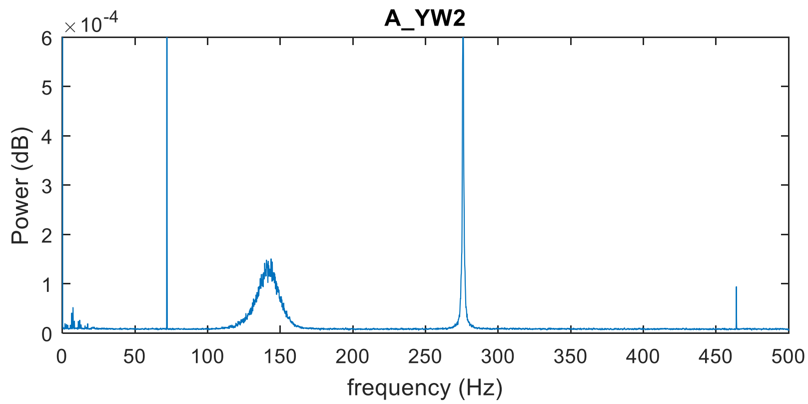
A_YW2
× 10^-4
Power (dB)
frequency (Hz)
0
50
100
150
200
250
300
350
400
450
500
0
1
2
3
4
5
6

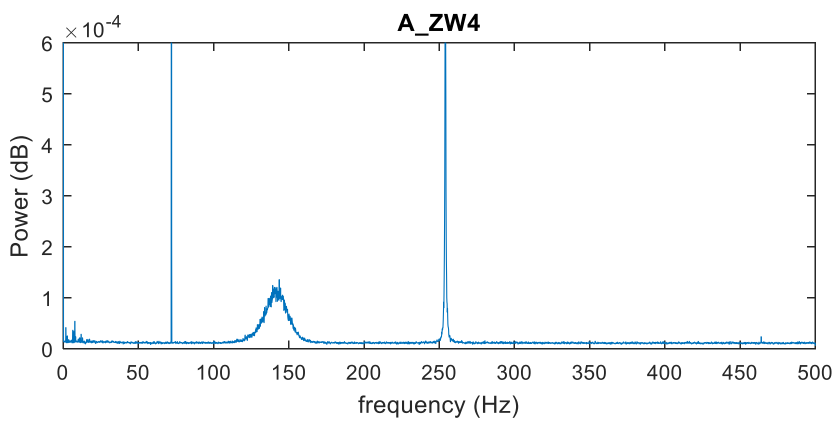
A_ZW4
× 10^-4
Power (dB)
frequency (Hz)
0
50
100
150
200
250
300
350
400
450
500
0
1
2
3
4
5
6

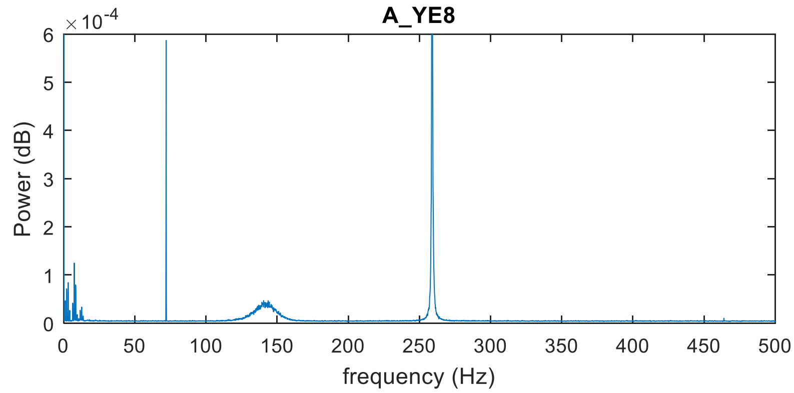
A_YE8
×10^-4
6
5
4
3
2
1
0
Power (dB)
0
50
100
150
200
250
300
350
400
450
500
frequency (Hz)

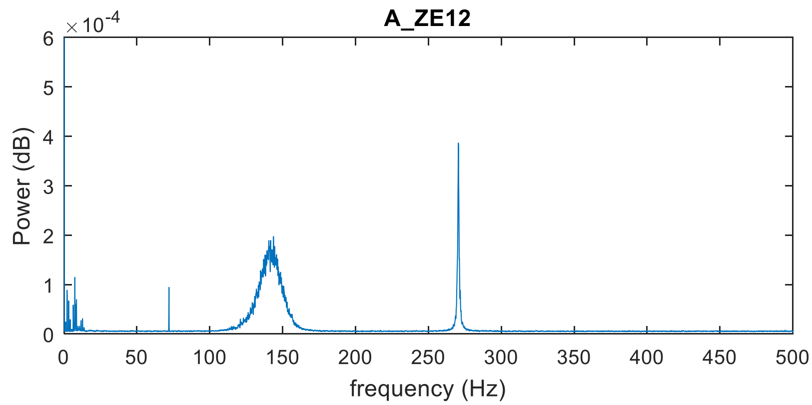
A_ZE12
×10^-4
6
5
4
3
2
1
0
Power (dB)
0
50
100
150
200
250
300
350
400
450
500
frequency (Hz)

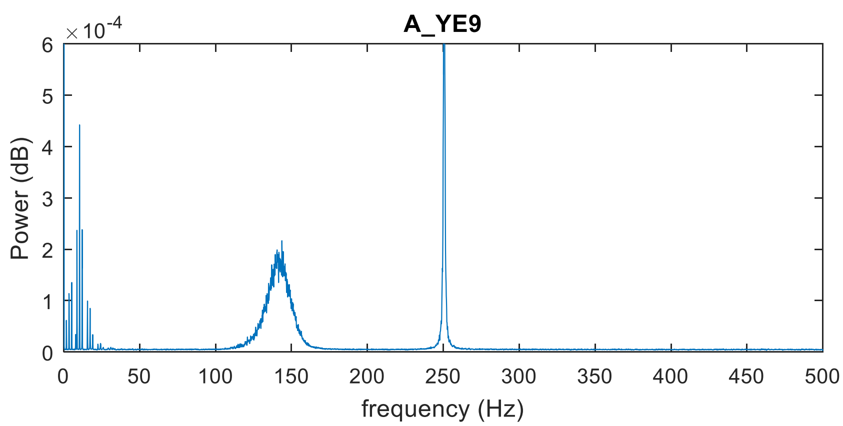
A_YE9
×10^-4
6
5
4
3
2
1
0
Power (dB)
0
50
100
150
200
250
300
350
400
450
500
frequency (Hz)

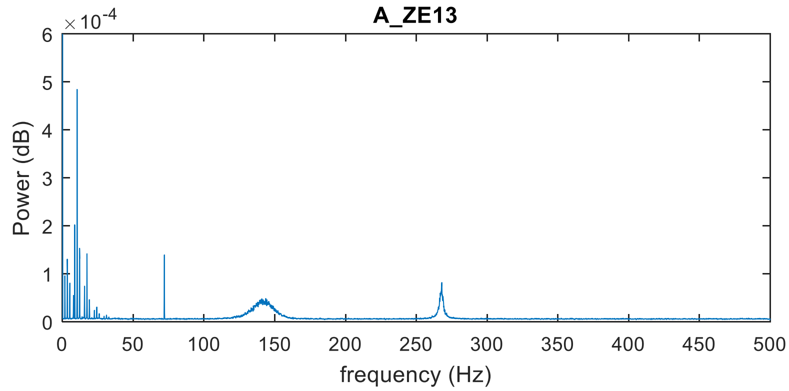
A_ZE13
×10^-4
Power (dB)
frequency (Hz)

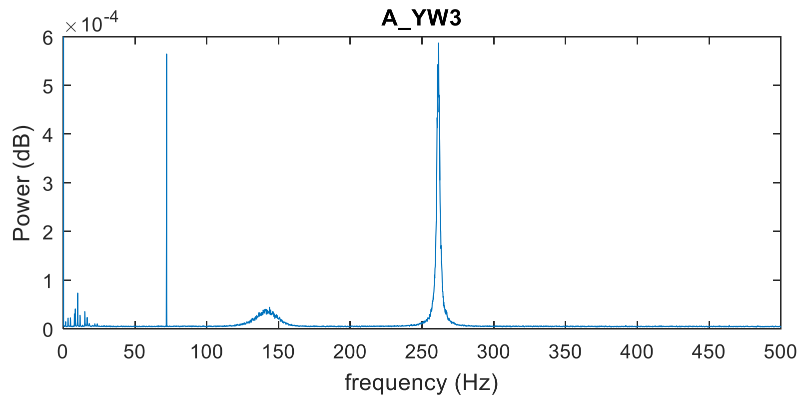
A_YW3
×10^-4
Power (dB)
frequency (Hz)

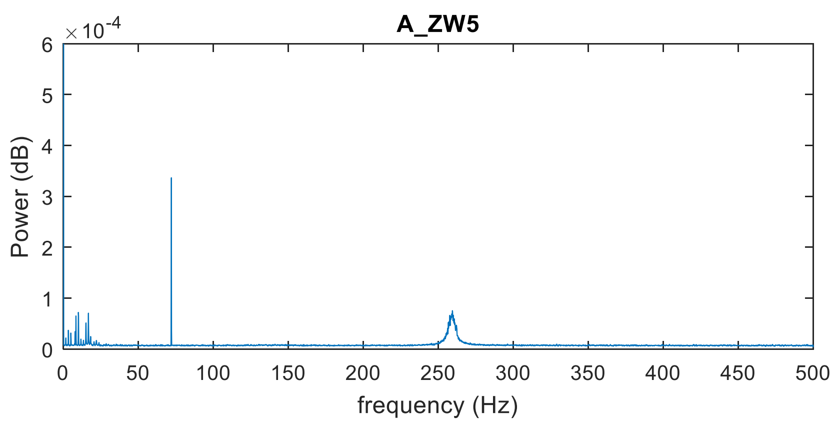
A_ZW5
×10^-4
Power (dB)
frequency (Hz)

`

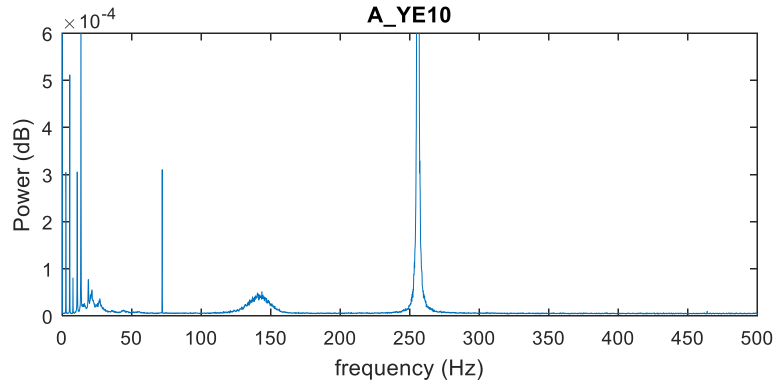
A_YE10
×10^-4
Power (dB)
frequency (Hz)

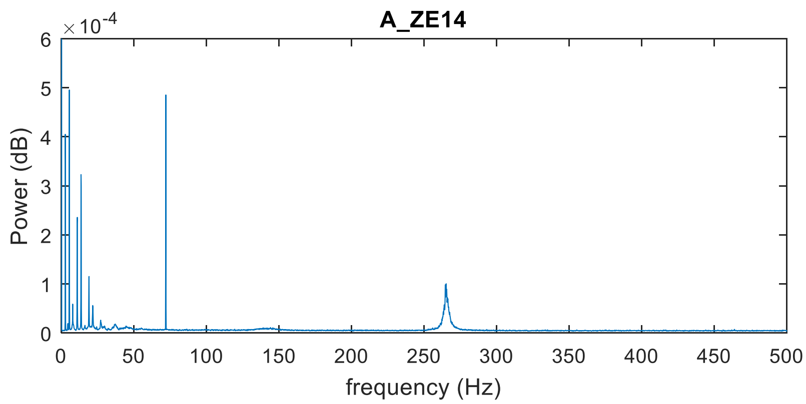
A_ZE14
×10^-4
Power (dB)
frequency (Hz)

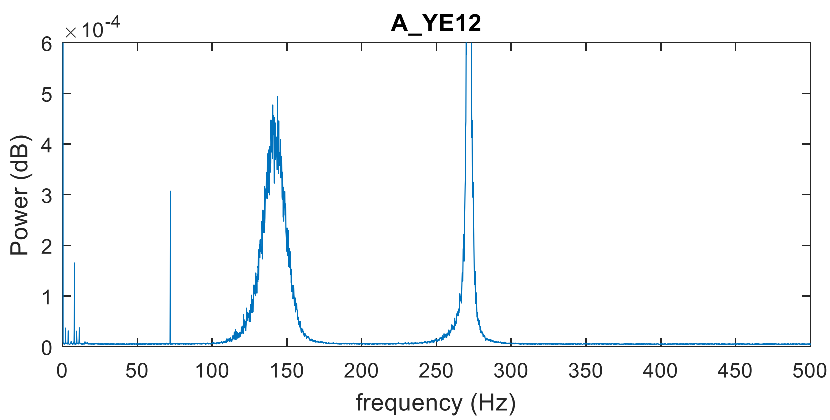
A_YE12
×10^-4
Power (dB)
frequency (Hz)

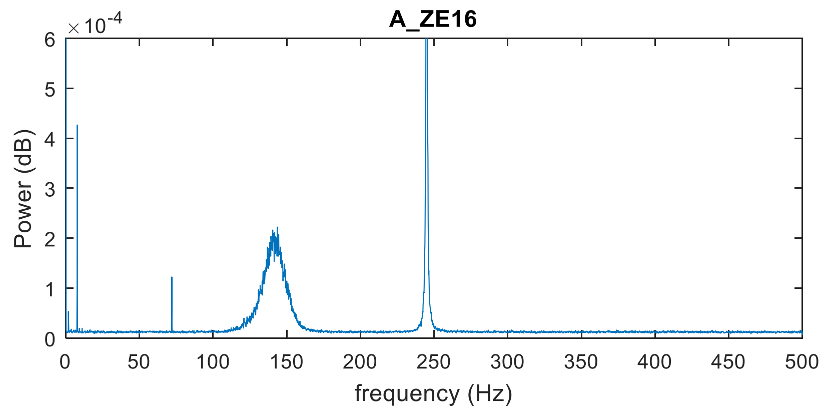
A_ZE16
×10^-4
Power (dB)
frequency (Hz)

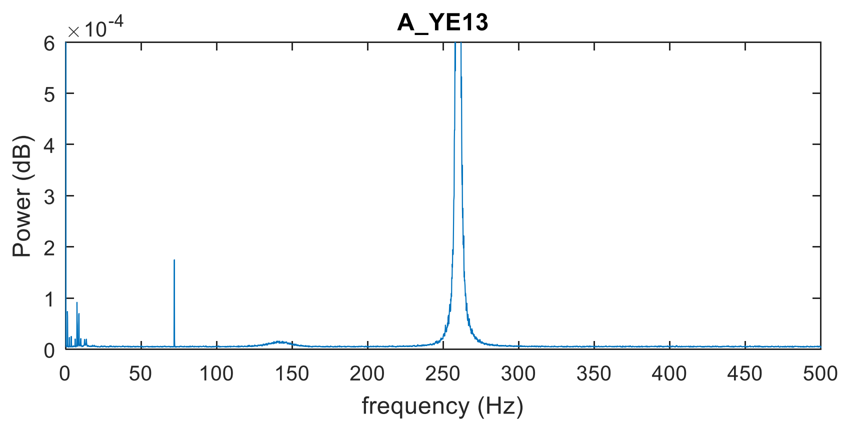
A_YE13
×10^-4
Power (dB)
frequency (Hz)

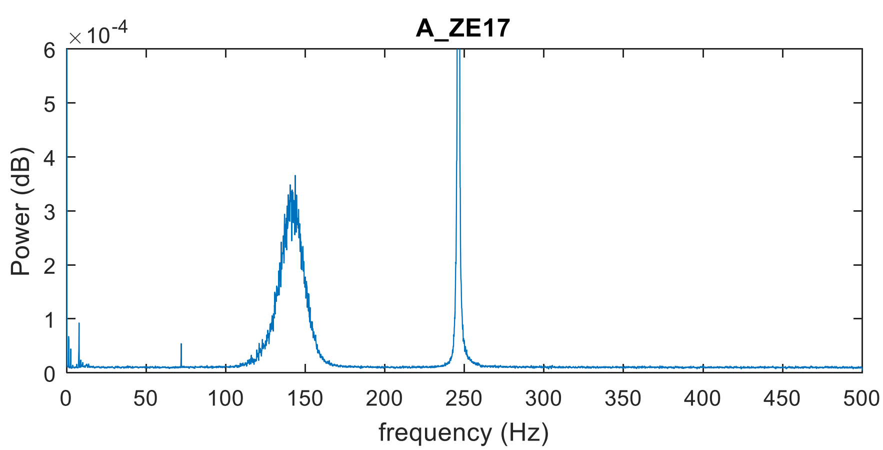
A_ZE17
×10^-4
Power (dB)
frequency (Hz)

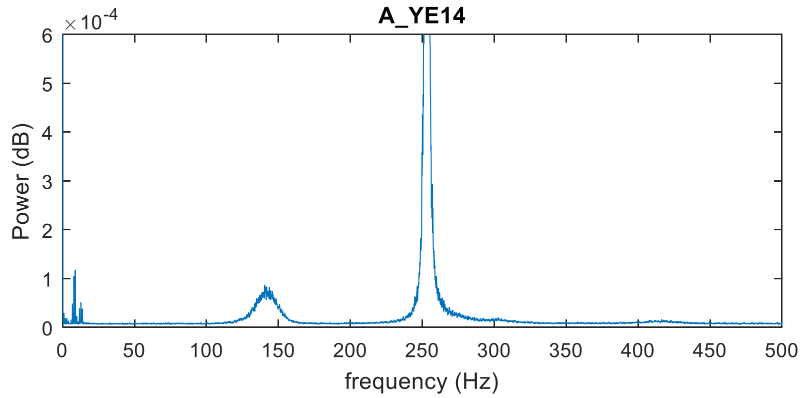
A_YE14
×10^-4
Power (dB)
frequency (Hz)
0
50
100
150
200
250
300
350
400
450
500
0
1
2
3
4
5
6

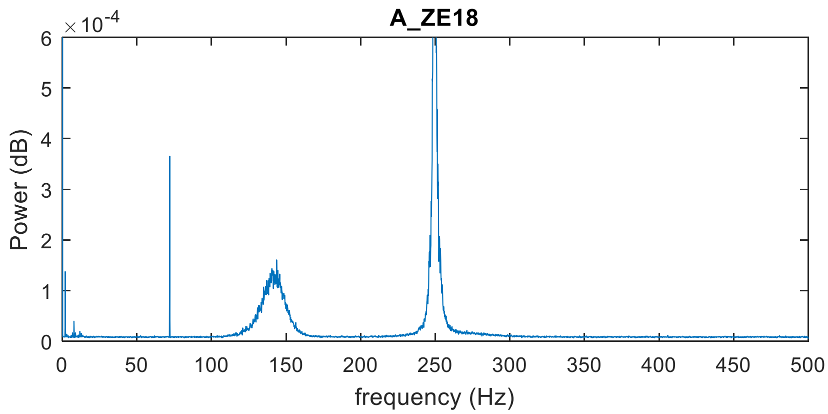
A_ZE18
×10^-4
Power (dB)
frequency (Hz)
0
50
100
150
200
250
300
350
400
450
500
0
1
2
3
4
5
6

Appendix B

MATLAB CODE

```
%read data from xlsx file
clc
clear all
close all
filename = '*.xlsx';%'My data has headers' should be selected, when
the data is exported from text file into Excel Worksheet
delimiterIn = ' ';
headerlinesIn = 1;
A = importdata(filename,delimiterIn,headerlinesIn);
 %for spesific col. For example col. 2
 %     for k =[2,2];
 %     disp(A.colheaders{1, k})
 %     disp(A.data(:, k));
 %     end
 for  count=1:size(A.colheaders,2)
     assignin('base',genvarname(A.colheaders{count}),A.data(:,count))
 end



 % Clean nan sampling and analysis data
 Indicators=
{'A_YE6','A_ZE10','A_YE7','A_ZE11','A_YW2','A_ZW4','A_YE8','A_ZE12','
A_YE9','A_ZE13','A_YW3','A_ZW5','A_YE10','A_ZE14','A_YE11','A_ZE15','
A_YE12','A_ZE16','A_YE13','A_ZE17','A_YE14','A_ZE18'}';% the
Indicators names of acceleration sensors on the cables
 mass = [1.47528, 1.47528,1.47528,1.47528, 1.47528,1.47528,
1.008108,1.008108, 0.885168,0.885168, 0.885168,0.885168,
0.6147,0.6147, 0.590112,0.590112, 0.811404, 0.811404,0.934344,
0.934344, 1.499868,1.499868]; % the mass per unit length (s/ft) for
the cables
 leng = [505,505,505,505, 505, 505, 407.4,407.4, 287,287,287, 287,
171.7, 171.7, 154.8,154.8, 246.6, 246.6,367.3, 367.3,458.9,458.9];
%the length of the cables (ft)
 Design_Tensions=[1438 1438 1432 1432 1390 1390 768 768 758 758 758
758 576 576 491 491 688 688 934 934 1127 1127]'; % the tensions at
the end of construction for each cable
 cables={'219E_Y','219E_Z','319E_Y','319E_Z','319W_Y','319W_Z',
'315E_Y','315E_Z','310E_Y','310E_Z','310W_Y','310W_Z','305E_Y','305E_
Z','404E_Y','404E_Z','408E_Y','408E_Z','413E_Y ','413E_Z
','419E_Y','419E_Z'};
 %Specific threshold should be used to determine the fundamental
frequency(this threshold is not constant)
```

```
 thresh_hold=[1.7 2 2.5 1.7 2.5 1.7 2.5 2 1.7 2 1.7 2 1.7 2 2 2 2.5 2
2.5 1.7 5 1.7]; %if there is no result show up for specific cable,
the threshold should be adjusted for that cable.

Tension_Force_using_Taut_Cable_Theory_Kips=zeros(length(Indicators),1
);

the_difference_between_masured_design_tension=zeros(length(Indicators
),1);
 for  count=1:length(Indicators)
            test_sensor=ismember(Indicators(count),A.colheaders);%
test each sensor if it has data in the file or not
    if      test_sensor==1
            test_var = eval(Indicators{count});
            average = nanmean(test_var);% find the average of all
data without nan
            indexnan=find(isnan(test_var)); % find the index of the
nan
            %if the entire column is 'NaN', replace it by 0
                    if isnan(average)
                       average=0;
                   end
            test_var(indexnan)=average;
     if     average~=0 % this 'if loop' is used to skip the sensors
which do not have data
            [power,F]=pwelch(test_var,8192,4096,[],167); %convert the
data from time domain to frequency domain
            l=find(F>15); % Find the first 15 points of the
frequencies
            F(l)=[];
            power(l)=[];
            avarage1=mean(power(3:end)); % find the average of all
the peaks 'reference line'
            [allpeks,alllocs]=findpeaks(power(3:end));  % find all
the peaks
            [Max,~] = max(allpeks); % find the max. peak
            difference=Max-avarage1;% find the difference between the
average and max( might be beneficial for threshold)
            name = 'ACCLEROMETER_INDICATORS=';
            X = [name,Indicators{count}];
            disp(X)
           % ACCLEROMETER_INDICATORS= Indicators{count}
            [peks1,locs1]=
findpeaks(power(3:end),'Npeaks',1,'MinPeakHeight',avarage1*thresh_hol
d(count)); % find the first peak because the fundemantal frequancy
gives the first largest respond so i can use it to find other
frequancis
            f1=F(locs1); % find the location of the first frequancy
to use it as a min peak distance
           if f1<3 && f1>=0.4
            [pks,locs]= findpeaks(power(locs1-3:end),F(locs1-
3:end),'Npeaks',6,'MinPeakDistance',abs(f1-round(0.2*(f1))));
```

```
            fn=locs; % I have to figure out way that tells matlab if
you did
            % not find peaks with the hight that I give you, give me
emtey
            %cell or not clear but don't skip this location
            n=fn/fn(1);% frequency rate
            figure(count)
            plot(F(3:end),power(3:end))
            title( num2str(Indicators{count}));xlim([0 15]); ylim([0
0.0025])
            xlabel('frequency')
            ylabel('Power')
            hold all
            %  by usin frequancy rate, test if the frequancies
correct or not by using
            %  the logic fn=n* f1.... n=fn/f1
            disp('All frequencies')
                b=zeros(length(fn),1);
                z=zeros(length(fn),1);
                d=zeros(length(fn),1);
                for a=1:length(fn);
                    s=(round(fn(a)/fn(1)))-(fn(a)/fn(1));
                    if  s<=0.2&& s>=-0.2
                    L=['f(' num2str(round(fn(a)/fn(1))) ') = '
num2str(fn(a))];
                    disp(L);
                    b(a)=fn(a);
                    d(a)=pks(a);
                    elseif  s>=0.2 | s<=-0.2
                        L=['f(' num2str(a) ') = not correct
frequency'];
                         disp(L)
                      z(a)=fn(a);
                    end
                end
            frequancies=b(find(b));
            [~,index]=ismember(frequancies,F);
            [~,index1]=ismember(locs,F);
            [~,index3]=ismember(z,F);
            d= nonzeros(d);
            %find just the frequancies that I am intersted in
            disp('clear frequencies')
                c=zeros(length(frequancies),1);
                  for i=1:length(frequancies)
                      if d(i)>avarage1*2
                        L=['f('
num2str(round(frequancies(i)/frequancies(1))) ') = '
num2str(frequancies(i))];
                        disp(L)

c(i)=(4*mass(count)*(leng(count))^2*(frequancies(i)/round(frequancies
(i)/frequancies(1)))^2)/1000;
```

```
                        p1=
plot(F(index(i)),power(index(i)),'.g','markersize',24);
                        elseif  d(i)<=avarage1*2
                        L=['f('
num2str(round(frequancies(i)/frequancies(1))) ') = not clear-low
amplitude'];
                        disp(L)
                      end
                  end
            name = 'avarage_tension=';
            Q = [name,num2str(round(mean(nonzeros(c))))];
            disp(Q)

Tension_Force_using_Taut_Cable_Theory_Kips(count)=round(mean(nonzeros
(c)));
            name = 'design_tensionn=';
            W = [name,num2str(Design_Tensions(count))];
            disp(W)
            p2=  plot(F(index3),power(index3),'.y','markersize',24);
            p3=  plot(F(index1),power(index1),'.r','markersize',12);
           legend([p1,p2,p3],'clear and correct frequencies
','incorrect frequencies','All frequencies that have been picked')
           legend('boxoff')
            end
     end
      the_difference_between_masured_design_tension(count)=((abs(
Tension_Force_using_Taut_Cable_Theory_Kips(count)-
Design_Tensions(count))/Tension_Force_using_Taut_Cable_Theory_Kips(co
unt))*100);
     test_var = [];
    end

end


    T = table(Indicators,Tension_Force_using_Taut_Cable_Theory_Kips,

    Design_Tensions,the_difference_between_masured_design_tension,

                          'RowNames',cables)
```

Appendix C

VIBRATION GRAPHS FOR THE DATA FROM WINTER STORM JONAS, JANUARY 2016 AT 52.3 MPH

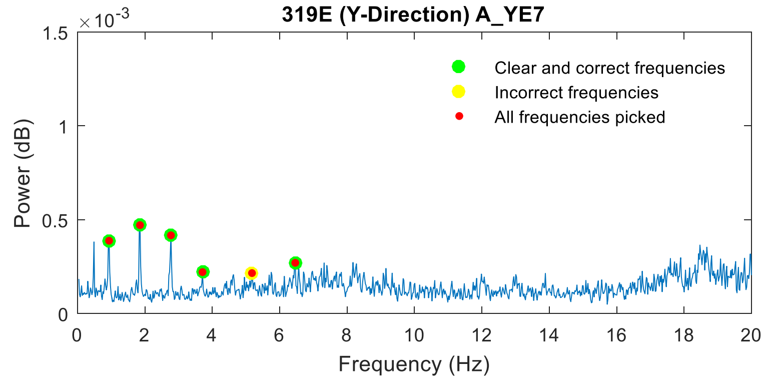

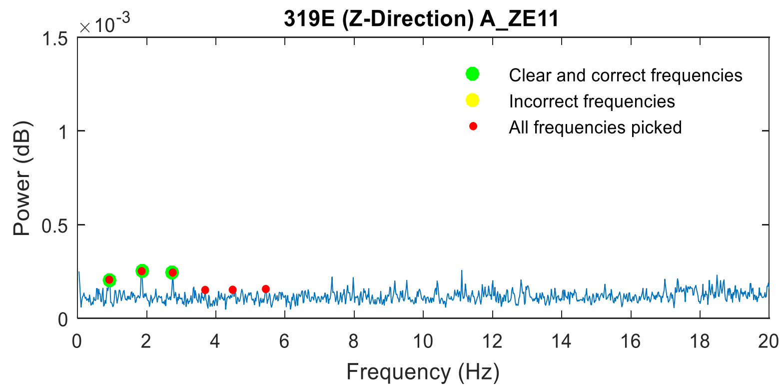

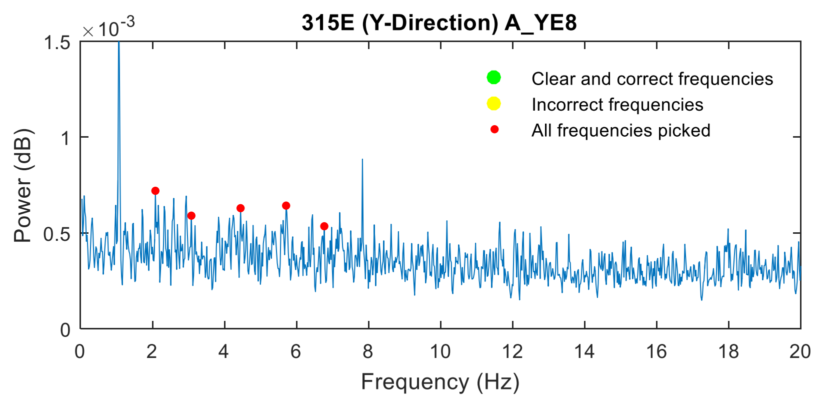

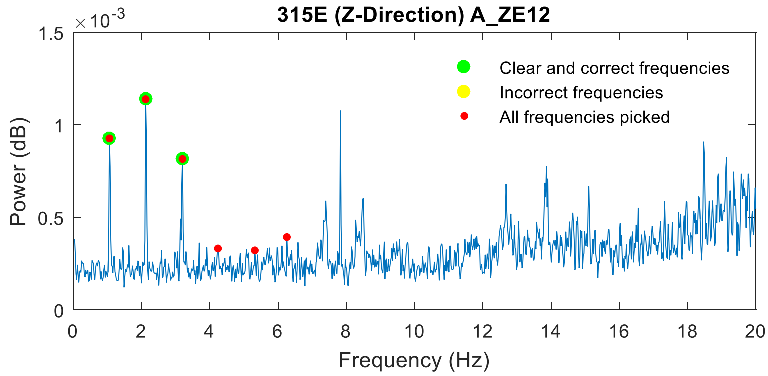
315E (Z-Direction) A_ZE12
×10-3
Clear and correct frequencies
Incorrect frequencies
All frequencies picked
Power (dB)
Frequency (Hz)

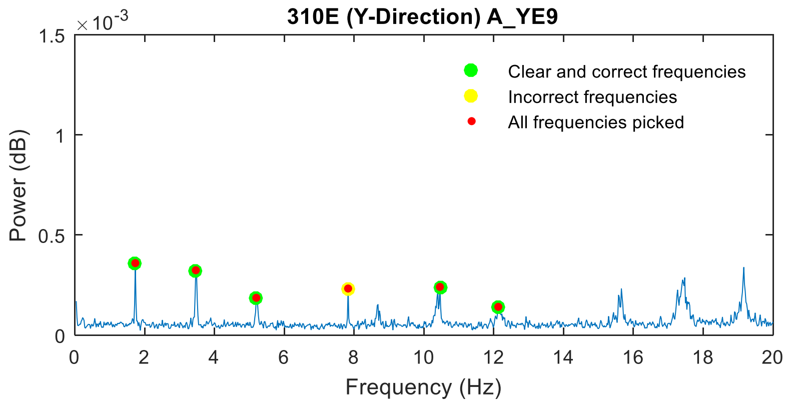
310E (Y-Direction) A_YE9
×10-3
Clear and correct frequencies
Incorrect frequencies
All frequencies picked
Power (dB)
Frequency (Hz)

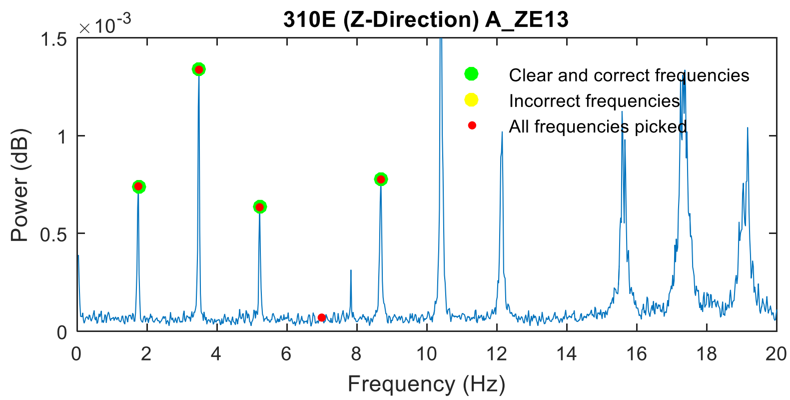
310E (Z-Direction) A_ZE13
×10-3
Clear and correct frequencies
Incorrect frequencies
All frequencies picked
Power (dB)
Frequency (Hz)

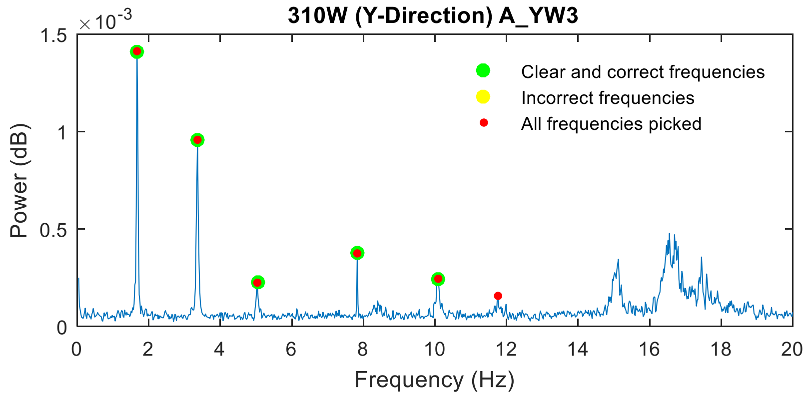
310W (Y-Direction) A_YW3
Clear and correct frequencies
Incorrect frequencies
All frequencies picked
Power (dB)
Frequency (Hz)

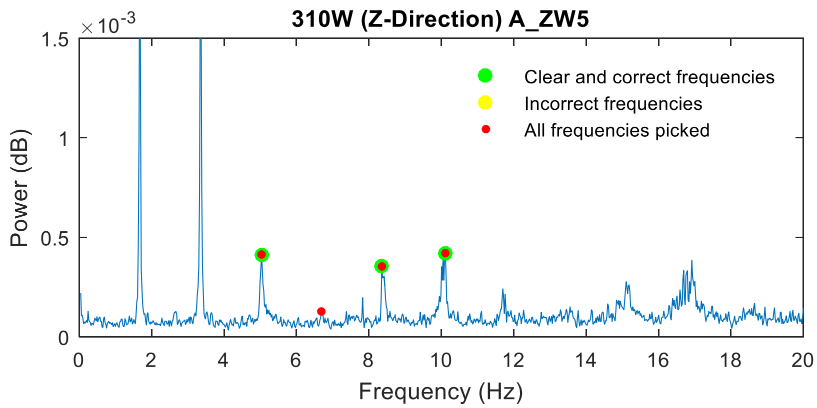
310W (Z-Direction) A_ZW5
Clear and correct frequencies
Incorrect frequencies
All frequencies picked
Power (dB)
Frequency (Hz)

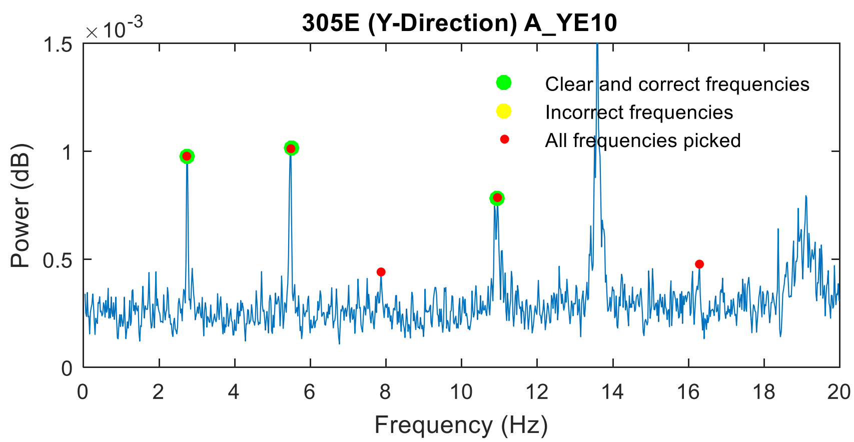
305E (Y-Direction) A_YE10
Clear and correct frequencies
Incorrect frequencies
All frequencies picked
Power (dB)
Frequency (Hz)

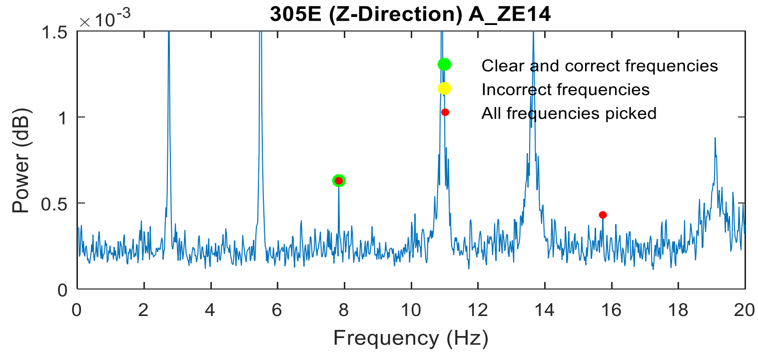

305E (Z-Direction) A_ZE14
Power (dB)
Frequency (Hz)
Clear and correct frequencies
Incorrect frequencies
All frequencies picked

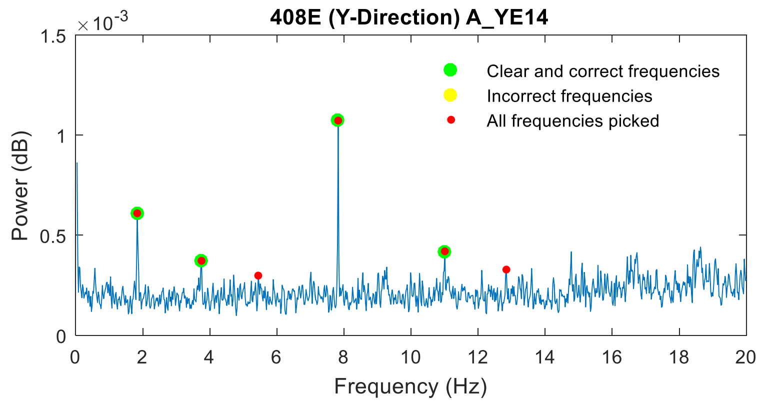

408E (Y-Direction) A_YE14
Power (dB)
Frequency (Hz)
Clear and correct frequencies
Incorrect frequencies
All frequencies picked

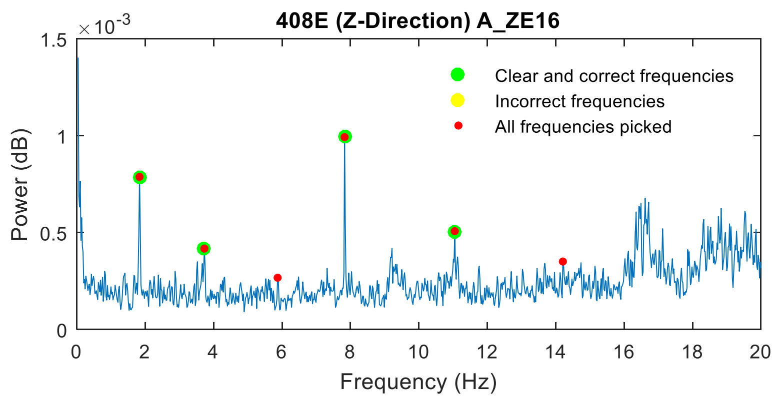

408E (Z-Direction) A_ZE16
Power (dB)
Frequency (Hz)
Clear and correct frequencies
Incorrect frequencies
All frequencies picked

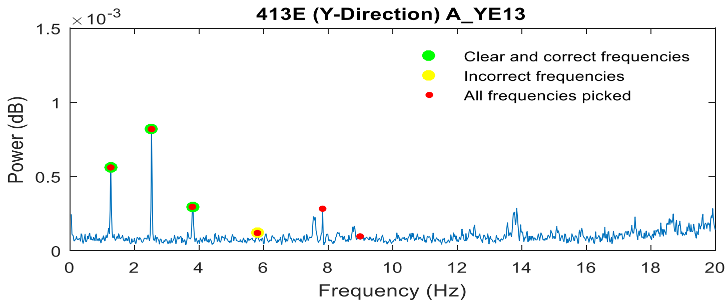
413E (Y-Direction) A_YE13
Clear and correct frequencies
Incorrect frequencies
All frequencies picked
Power (dB)
Frequency (Hz)

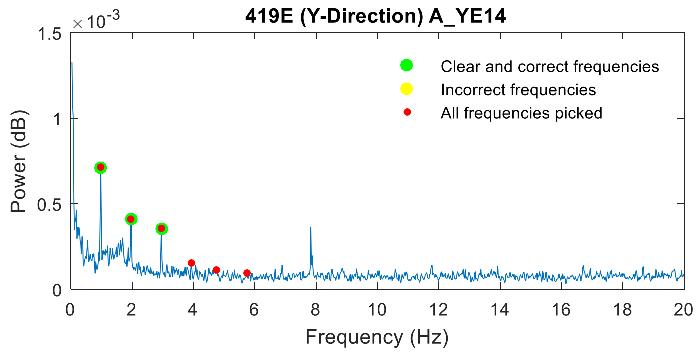
419E (Y-Direction) A_YE14
Clear and correct frequencies
Incorrect frequencies
All frequencies picked
Power (dB)
Frequency (Hz)

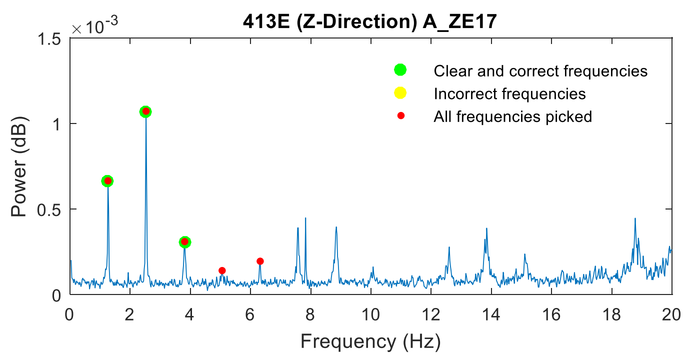
413E (Z-Direction) A_ZE17
Clear and correct frequencies
Incorrect frequencies
All frequencies picked
Power (dB)
Frequency (Hz)

`

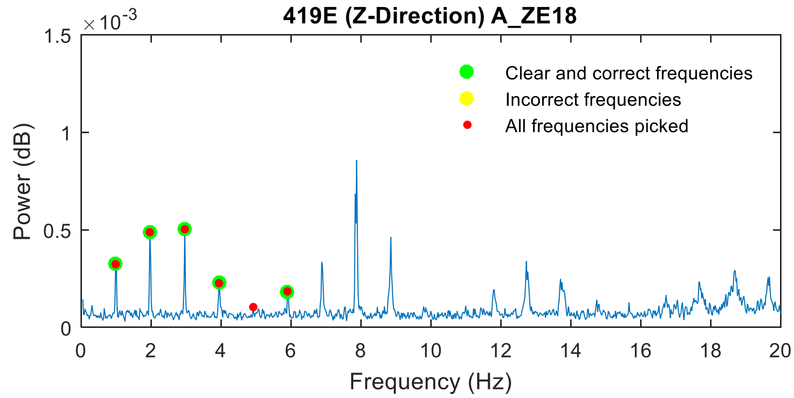

419E (Z-Direction) A_ZE18
×10^-3
1.5
1
0.5
0
Power (dB)
Clear and correct frequencies
Incorrect frequencies
All frequencies picked
0
2
4
6
8
10
12
14
16
18
20
Frequency (Hz)